University of Illinois at Urbana-Champaign

ACRC

Air Conditioning and Refrigeration Center A National Science Foundation/University Cooperative Research Center

Capacity and Efficiency in Variable Speed, Vapor Injection and Multi-Compressor Systems

S. Jain and C. W. Bullard

ACRC TR-227 May 2004

For additional information:

Air Conditioning and Refrigeration Center
University of Illinois
Mechanical & Industrial Engineering Dept.
1206 West Green Street
Urbana, IL 61801

(217) 333-3115

Prepared as part of ACRC Project #148
Exploring Component and System Design Tradeoffs
C. W. Bullard, Principal Investigators

The Air Conditioning and Refrigeration Center was founded in 1988 with a grant from the estate of Richard W. Kritzer, the founder of Peerless of America Inc. A State of Illinois Technology Challenge Grant helped build the laboratory facilities. The ACRC receives continuing support from the Richard W. Kritzer Endowment and the National Science Foundation. The following organizations have also become sponsors of the Center.

Alcan Aluminum Corporation
Amana Refrigeration, Inc.
Arçelik A. S.
Behr GmbH and Co.
Carrier Corporation
Copeland Corporation
Daikin Industries, Ltd.
Delphi Thermal and Interior
Embraco S. A.
Fujitsu General Limited
General Motors Corporation
Hill PHOENIX
Honeywell, Inc.
Hydro Aluminum Adrian, Inc.
Ingersoll-Rand Company
Lennox International, Inc.
LG Electronics, Inc.
Modine Manufacturing Co.
Parker Hannifin Corporation
Peerless of America, Inc.
Samsung Electronics Co., Ltd.
Sanyo Electric Co., Ltd.
Tecumseh Products Company
Trane
Visteon Automotive Systems
Wieland-Werke, AG
Wolverine Tube, Inc.

For additional information:

Air Conditioning & Refrigeration Center
Mechanical & Industrial Engineering Dept.
University of Illinois
1206 West Green Street
Urbana, IL 61801

217 333 3115

Abstract

Air conditioning and refrigeration systems are designed to meet the load at some particular design conditions. At off-design conditions, the compressor is either cycled or a variable speed drive enables the compressor to run at a speed that matches the load. However, cycling can incur efficiency losses as large as 10-20% of total compressor power. Similarly, the variable speed compressors suffer from an efficiency penalty as a result of the losses in the inverter drive (4-6%).

Part 1 of this report focuses on the use of tandem compressors, that is, a combination of two or more compressors running in parallel with each other, to more closely match the load at different conditions. Simulation models were run for various operating conditions and the results from the tandem simulations were compared with the single speed and the variable speed compressor results, showing a significant COP over the single speed case and a smaller improvement over the variable speed case. Temperature data from Pittsburgh and Dallas was then incorporated, and the optimum compressor sizing and operating strategies were compared. Results again showed a COP gain of 7.5% and 6.2% for the two cities, respectively, over the case of a single-speed compressor, and 2.2% and 2.0% compared to a variable-speed compressor.

Part 2 focuses on vapor injection in case of scroll compressors used in air-conditioning and refrigeration applications. Vapor injection alters the normal refrigeration cycle by adding an injection port to the scroll compressor. After partial expansion upstream of the evaporator, refrigerant vapor is injected into the compressor. It saves compressor energy because that fraction of the flow needs only partial compression, and saves compressor volume because less vapor enters the suction port and the refrigerating effect increases due to the lower inlet quality. Simulation models were run for different operating conditions and it was discovered that for systems sized to meet the same design load, the VI systems had a higher COP of around 8-10%, for air-conditioning applications. Similarly for the refrigeration case, the VI system registered a COP increase of as much 16%. VI systems also helped in reducing the compressor displacement by around 25% in the air-conditioning and 30% in the refrigeration case respectively.

Table of Contents

List of Figures

Page

Nomenclature

Variables

T:	temperature (°C)
P:	pressure (kPa)
PR:	pressure ratio
h:	enthalpy (kJ / kg)
s:	entropy (kJ / kg-K)
m_{dot} :	mass flow rate (kg / sec)
Q:	load (kW)
W:	compressor work (kW)
V:	volume (m^3)
V_{dot}:	volumetric flow rate (m^3 / sec)
x:	dryness fraction
v:	specific volume (m^3 / kg)

Greek

η:	isentropic efficiency
η_{vol}:	volumetric efficiency
ω:	frequency (rev / sec)
μ :	run-time fraction
ρ:	density (kg/m^3)

Subscripts

CPin:	compressor inlet side
CPout:	compressor outlet side
CDin:	condenser inlet side
CDout:	condenser outlet side
EVin :	evaporator inlet side
EVout:	evaporator outlet side
LP:	low-pressure compressor
HP:	high-pressure compressor
EV:	evaporator conditions
vsd:	variable speed compressor
csd:	constant speed compressor
amb:	ambient conditions
load:	external load

Chapter 1: Introduction

This report explores the potential for compressor choices to meet sometimes conflicting demands for system capacity and efficiency. Specifically, the variable- and single-speed compressor combinations are examined and their capacity/efficiency tradeoffs quantified. Part II examines ways in which vapor-injected scroll compressors can be used to increase efficiency, and to obtain more capacity from a given displacement rate.

Air-conditioning or refrigeration systems are designed for certain standard design conditions (e.g. ARI-A). The compressors are sized such that the system is able to match the load at these points. However, with the change in ambient conditions, the load on the system would vary, while the system would continue to provide the capacity as is specified by the design point. For example, even at half load, the constant speed compressor would still be producing almost the same amount of refrigerating effect as it did in case of the full load. Hence we should try to design the system in a way such that it adapts itself with the changes in the ambient.

One way of achieving this is to cycle the single speed compressor for all conditions when the capacity exceeds the load. However, there are certain losses associated with cycling, which are in the range of 10-20% depending on the runtime fraction.

A variable speed drive is another way of matching the capacity of the system to the off-design load by modulating the refrigerant mass flow rate to change the evaporator capacity.

However the variable speed compressor encounters lubrication problems at low speeds, and has poor valve performance at very high speeds. It also suffers an efficiency penalty as a result of losses in the inverter drive (~4-6%). Hence we consider alternative methods for modulating mass flow, without sacrificing compressor efficiency, while minimizing cycling losses.

The second part of the report explores the benefits obtained through the use of vapor injection in scroll compressor applications. Vapor injection has also been employed with screw compressors, with an increase in both capacity and system COP. It divides the compression in two stages, reducing the compressor work, and lowers the inlet quality to the evaporator, thus improving capacity and COP. The question is whether the performance improvements are large enough to exceed the cost of additional components required.

Chapter 2 introduces the concept of tandem compressors and explains the basic fundamental. After the introduction, Chapter 3 describes the various components of the simulation model and the different assumptions and variables used in the development of the model. The chapter also discusses the different options considered in developing the optimal operating strategy for tandem compressors. The results are then discussed in Chapter 4, with both the 2 and the 3 compressor systems being considered. The next chapter deals with the seasonal efficiency considerations, and explains the results obtained when the simulation model is applied to real-time data systems. In this case we have analyzed the data obtained from the cities of Pittsburgh and Dallas. The conclusions for this part are then presented in Chapter 6. Appendix A discusses the change in the results obtained by using the new expression for the cycling loss factor.

Part 2 of the project, which deals with vapor injection in scroll compressors, is covered in the subsequent chapters. Chapter 7 describes the application of vapor injection in scroll compressors, with the next chapter dealing with an ideal cycle analysis for vapor injection systems, and explains the benefits obtained through it. Chapter 9

discusses the simulation model used in the analysis and its development. It also deals with the model developed for simulating the compression process inside the scroll compressors and the various losses associated with it. The validation of the compressor model is also a part of this chapter. Chapter 10 details the results obtained when the model is applied to air-conditioning applications and presents the efficiency and capacity comparisons between the vapor injection and the base case. Chapter 11 describes the results for the refrigeration applications, and the conclusions are then presented in Chapter 12.

Appendix B starts with the comparison between the ideal flash tank and ideal heat exchanger models, and then compares the ideal and real systems. Appendix C describes the new developments in scroll compressor technology and the expected change in results obtained due to these developments. Appendix D quantifies the COP gains obtained through the use of vapor injection using different refrigerants.

Chapter 2: Tandem Compressors

Consider the use of tandem compressors in place of a single speed or variable speed compressor. Using a combination of two or more compressors, running in parallel to each other, operated individually and together, the system is able to match a wide range of load requirements. The objective is to minimize the power consumption and thus maximize efficiency, while being able to match the ambient load.

To start with, we consider a combination of two compressors, a variable speed and a single speed compressor. The model will then be generalized to 3 or more compressors to identify configurations having the highest efficiency. Then it will be used to identify the optimal combination of displacement volumes for managing system efficiency while covering the entire load range. The system is shown schematically in Figure 2.1.

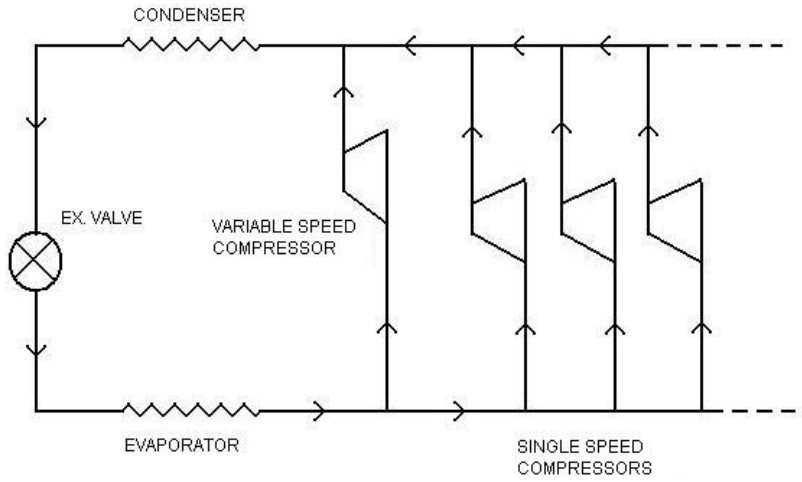

Figure 2.1 Schematic of the tandem compressor model

Distributing the refrigerant flow rate between the two compressors in different ways enables us to generate a performance plot of our system, and help quantify trade-offs in optimizing the system efficiency. The refrigerant leaves the evaporator and then gets divided between the two compressors, proportional to their displacement rates. It then passes onto the condenser and then through the expansion valve it returns back to the evaporator and the cycle is completed. Using the state points as described above, the cycle can be represented on the p-h diagram as shown in Figure 2.2. The two different lines for the compression process indicate the presence of two compressors, and the fact that these compressors are operating at different efficiencies.

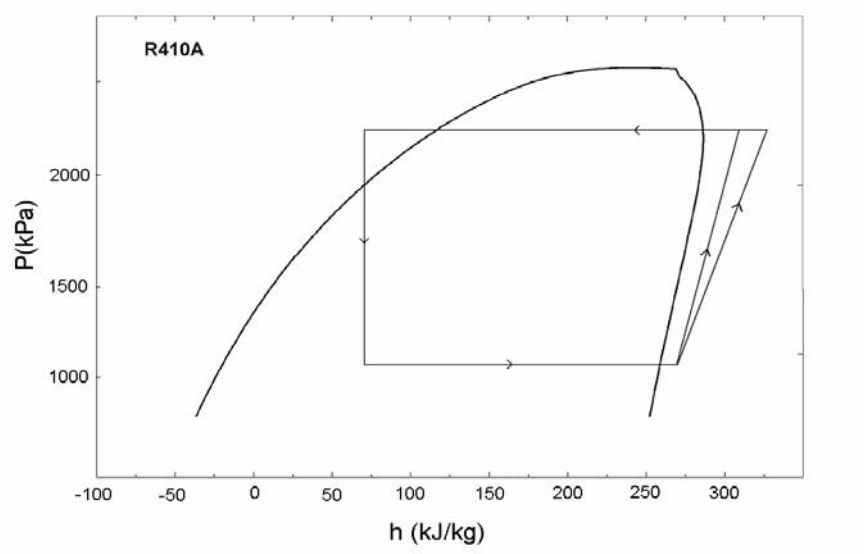

Figure 2.2 P-h diagram of the tandem compressors cycle

Chapter 3: Simulation Model

In tandem compressors system, for the variable speed compressor, we assume that the speed can vary from 1800 rpm to 6600 rpm (30 – 110 Hz). The other compressor operates at 3600 rpm (60 Hz). This is the speed at which the compressor operates with the maximum mechanical and motor efficiency. For this model we neglect variations in volumetric efficiency.

The isentropic efficiency of the compressor (η_{isen}) varies with the pressure ratio between the condenser and the evaporator, as well as with the compressor speed. We assume that the efficiency has a linear relation [1] with the pressure ratio and that it has a value of 0.7 at a pressure ratio of 1.5 and 0.65 at a ratio of 2.5). The relation is given by the following expression.

$$\eta = (-0.05) * (PR) + 0.775 \quad (1)$$

Also, over this speed range (30 - 110Hz) the isentropic efficiency varies as a quadratic function of speed [2], and this fact has been taken into account by normalizing the efficiency term for a speed of 60 Hz, and is represented by the following equation.

$$\eta_{\omega} / \eta_{\omega 60} = -0.08 * (\omega / \omega_{60})^2 + 0.1411 * (\omega / \omega_{60}) + 0.9337 \quad (2)$$

The overall isentropic efficiency of the compressor is then given by the product of these two expressions. Figure 3.1 shows the variation of η_{isen} with the pressure ratio.

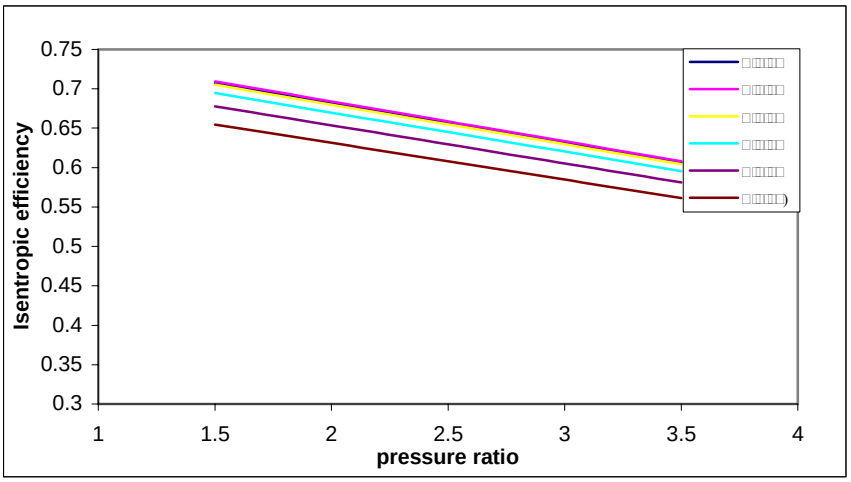

Figure 3.1 Isentropic efficiency as a function of pressure ratio at different speeds

Another important consideration is that, for the case of the variable speed compressor, we assume that it is running on an inverter drive, with electrical losses of 4% upstream of the compressor. [3]

Also, while calculating for the COP, the cycling losses must be taken into account. As defined by the ARI standards [4], these losses are approximated by a multiplicative factor C_d applied to the COP term. The expression for this factor is given as follows.

$$C_d = 0.8 + 0.2 * \mu \quad (3)$$

where, μ is the run-time fraction.

Next, instead of modeling a condenser with a particular geometry, it is assumed that the condenser's entering temperature difference is 10°C at the ARI-A (T_{amb} = 35°C) design condition, and varies linearly with ambient temperature.

$$T_{CDin} = T_{amb} + 10 * (Q_{cond} / (W_{total} + (Q_{load})_{des}))$$

or,

$$T_{CDin} = T_{amb} + 10 * ((W_{total} + Q_{evap}) / (W_{total} + 10.5)) \quad (4)$$

Q_{cond} is the condenser heat rejection and Q_{evap} is the evaporator capacity. The expansion valve is assumed to be isenthalpic in nature. For the evaporator we choose the overall UA value in a manner such that, at the design point, the T_{evap} is 12°C. The base model is then used with this fixed evaporator geometry (UA) and the T_{evap} is maintained at 12°C by changing the mass flow rate of air over the evaporator.

Next, Q_{load} is assumed to vary linearly with ambient temperature from zero at an ambient temperature of 18C, to 10.5 kW at the design outdoor temperature of 35°C. For an actual building, loads will vary around this line due to radiative gains through windows, and due to latent and internal loads, but for purposes of this analysis, the equation can be taken to represent the mean at any ambient temperature, and is represented in Figure 3.2.

$$Q_{load} = (10.5 / (35 - 18)) * (T_{amb} - 18) \quad (5)$$

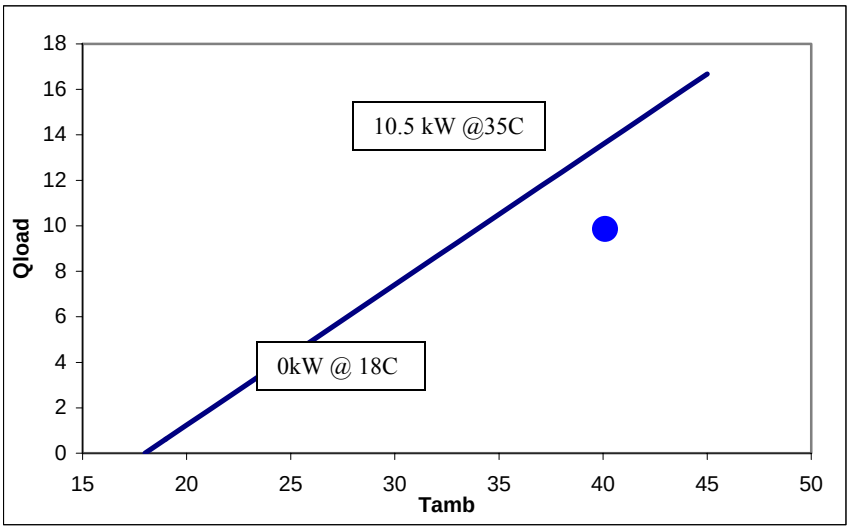

Figure 3.2 Load variation with ambient temperature T_{amb}

Also, we define a variable F_v as,

$$F_v = V_{vsd} / V_{total}$$

Where, V_{vsd} = displacement volume of the variable speed compressor,

V_{total} = sum of the volumes of the single speed and the variable speed compressors

Finally, the R410A cycle is completed by assuming 5°C superheat at the evaporator exit and 5°C subcooling at the condenser exit.

3.1 Optimal sizing and operating strategy

The total displacement volume is determined by matching the load at an (arbitrarily selected) design ambient temperature of 35°C, assuming that both the compressors are running at 60 Hz. Next, we try to identify the F_v value that would maximize COP over a wide range of operating conditions, as illustrated by the following simplified analysis.

This simple relationship shown in Figure 3.3 implies that at the ARI-A design condition, the COP of the system is maximum when $F_v = 0$, or when we have only the single speed compressor. This reflects the inverter drive loss, which is present in case of the variable speed compressor only.

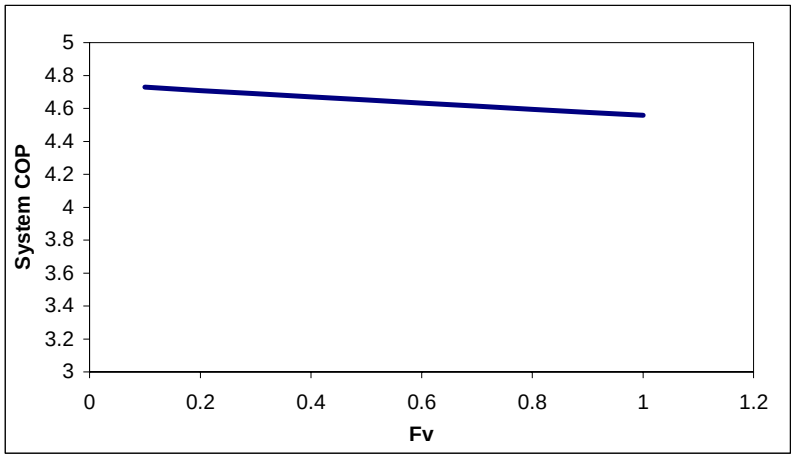

Figure 3.3 COP as a function of F_v for the ARI-A design condition

However, we are looking for a system that would be able to cover the cooling loads for an entire range of ambient temperatures. For values of F_v less than 0.5 cycling is required for meeting certain ranges of the load. The lower the value of F_v, the greater the range of operating conditions in which we have to incur cycling losses, as illustrated in Figure 3.4.

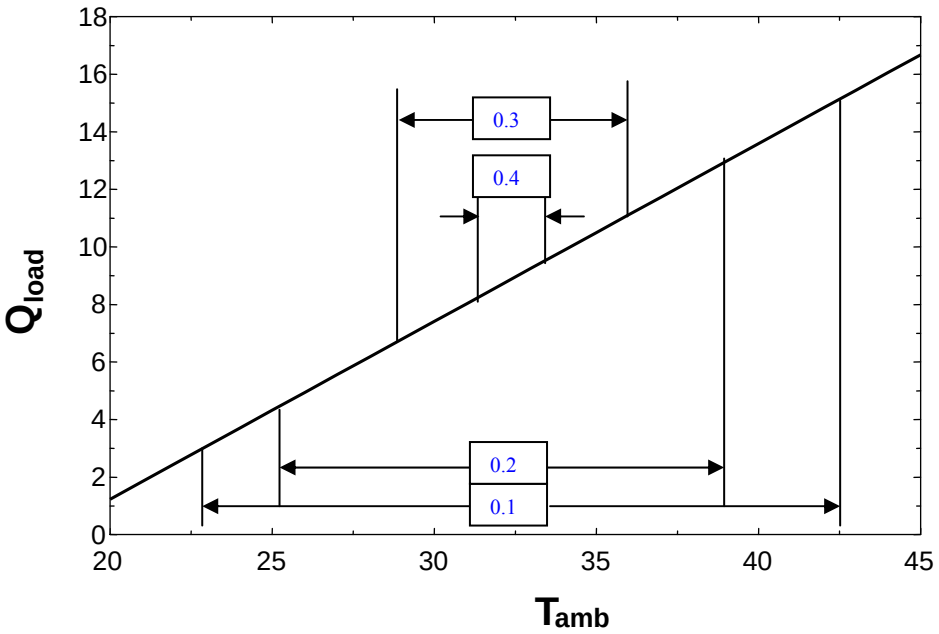

Figure 3.4 Intervals where cycling is required for a 2-compressor system

Figure 3.4 shows the temperature ranges in which we shall have to employ cycling. The values in boxes represent the F_v values. For lower values of F_v (<0.4) the cycle-off range is large, and results in large cycling losses. For larger values of F_v (>0.6), the large variable speed compressor would be able to match a wide range of loads, but the inverter losses would be larger.

3.2 Option I

The variable speed compressor starts operating at its minimum speed of 30 Hz. The load is matched by cycling the variable speed compressor until the temperature reaches 22°C. With the rise in temperature, the speed of the variable speed compressor continues to increase to match the load, until the load reaches a point where it can be taken care of by the single speed compressor alone. At this point the variable speed compressor stops, and the single speed one takes over. However with the further rise in temperature, the variable speed compressor also starts operating in tandem with the single speed compressor and in this manner we are able to match all the loads.

However, at the point where the single speed compressor takes over, the variable speed compressor will be cycling again at its minimal speed of 30 Hz, until the ambient temperature rises to the point where the load exactly equals the capacity two compressors running in tandem. Thereafter, the compressor speed can be increased continuously to 110 Hz to track the highest loads without cycling. To gain further insight into this operating strategy, we analyze the load and capacity plots for different F_v values.

Figure 3.5 shows many points where the Q_{total} exceeds Q_{load}. These points define the range in which cycling must be employed. Similarly Figure 3.6 shows the case when $F_v = 0.5$, which reveals a smaller range of ambient temperature where cycling is required. This can be attributed to the larger VS compressor.

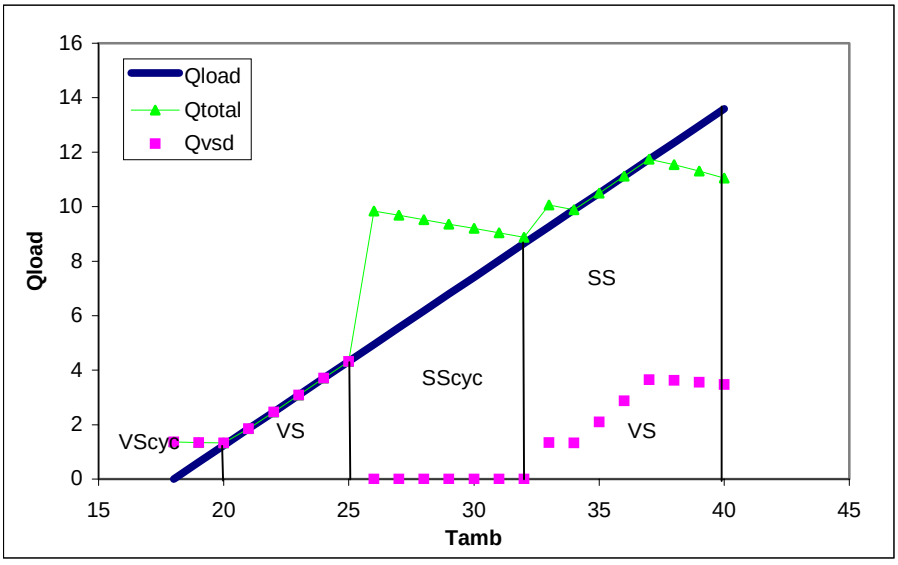

Figure 3.5 Load-capacity for varying T_{amb} curve for F_v=0.2

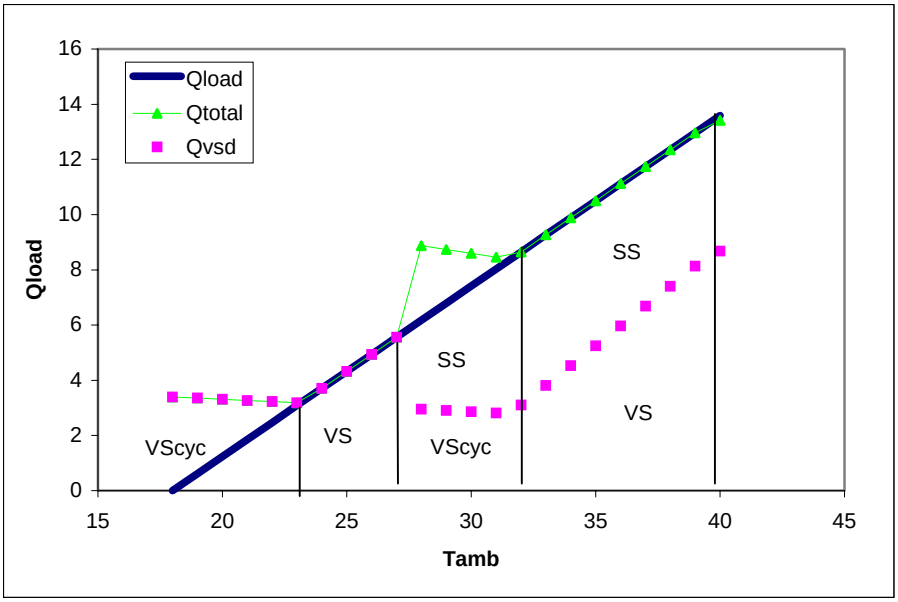

Figure 3.6 Load-capacity for varying T_{amb} curve for F_v=0.5

Increasing F_v to 0.7 as shown in Figure 3.7, the range of cycling conditions increases. Also, there would lower average system COP due to the larger inverter drive penalty.

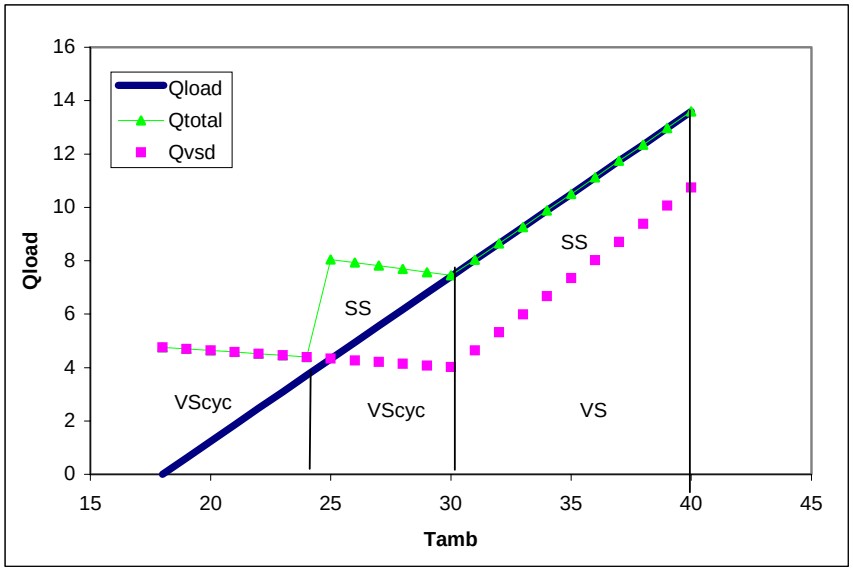

Figure 3.7 Load-capacity for varying T_{amb} curve for F_v=0.7

In general, if the compressors are operated in the manner as specified by Option 1, cycling will be necessary that for a significant amount (25-30%) of the load range.

3.3 Option II

Another strategy for running the compressors is, instead of stopping the variable speed compressor, and then shifting over to the constant speed one, to let the variable speed one follow the load by increasing its speed beyond 60 Hz, until the load increases to the point where it can be met by the single speed compressor plus the

variable speed one running at its minimum speed (30 Hz). At that point the constant speed compressor is switched on and the variable speed compressor is slowed to its lowest speed. With further rise in temperature the speed of the variable speed compressor increases to follow the load. In this manner we are able to minimize the cycling interval.

For the case of a small variable speed compressor shown in Figure 3.8, the VS cycles the temperature range 18-22°C, while the SS compressor is being cycled in the range 31-40°C.

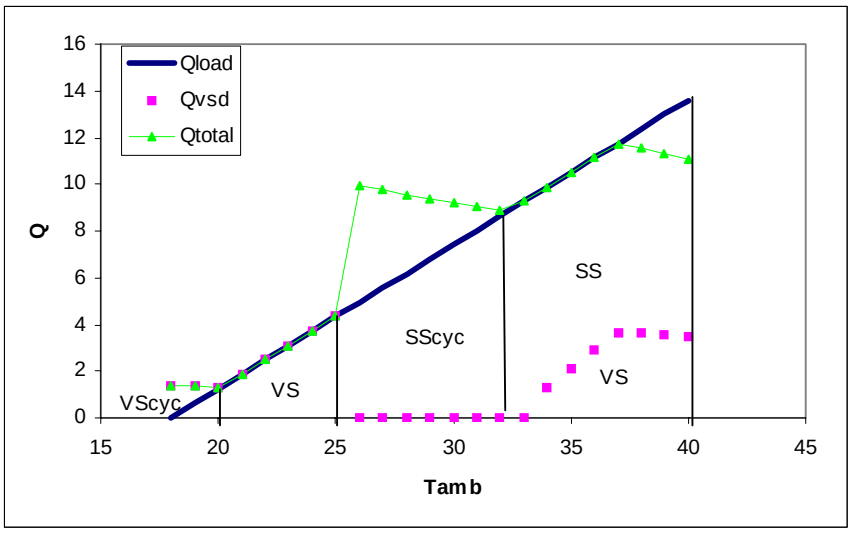

Figure 3.8 Load-capacity for varying T_{amb} curve for F_v=0.2 for option II

As the size of the variable speed unit increases to F_v = 0.45, cycling losses are traded for inverter losses as shown in Figure 3.9. Here we don't have to cycle the SS at all, and most of the loads are matched exactly except for a small region (18-25°C) where the VS compressor is cycling.

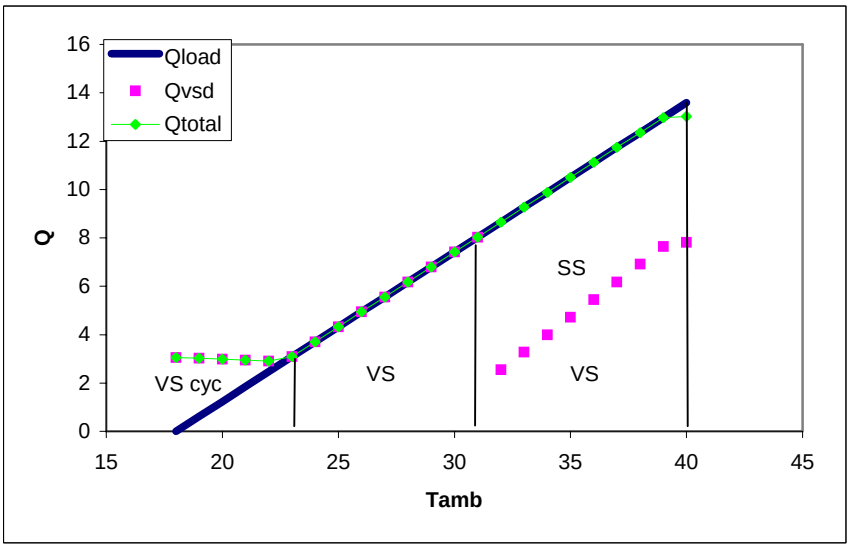

Figure 3.9 Load-capacity for varying T_{amb} curve for F_v=0.45 for option II

Similarly for the F_v = 0.7 case, the results are shown in Figure 3.10.

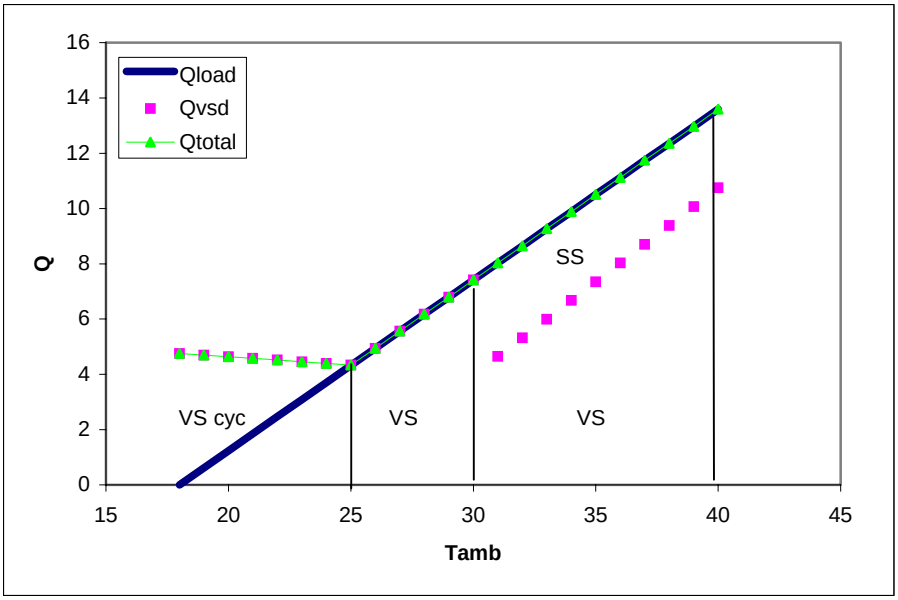

Figure 3.10 Load-capacity for varying T_{amb} curve for F_v=0.7 for option II

For this case the VS compressor cycling range increases to 18-29°C. As F_v continues to increase, so does the cycling. Similarly, for values of F_v<0.45, both compressors must be cycled more.

Chapter 4: Results

The results obtained from the simulation model are discussed below.

4.1 Optimal operating strategy for 2 compressor system

We have analyzed the two options for operating the tandem compressors, and on the basis of the Figures 3.5-3.10, it seems that since less cycling is required for Option II, it would prove to be the best way to run the compressors. However, running the model, and optimizing the COP for all the operating conditions, it was discovered that running the VS compressor in the speed range of 85-110 Hz, is less efficient than cycling it (cycling losses exceed the ~4% inverter loss). Hence the optimal strategy would be run the VS compressor initially, letting it run up to 90-95 Hz, and then allowing the SS compressor to kick in, with the VS cycling at 30 Hz. Eventually with increasing load, the VS also picks up speed and the compressors running in tandem match the load.

Recent evidence from ARI [5], based on experimental data, suggests that actual values of cycling losses are on the order of 10-12% for modern systems The trend towards more compact systems and improvements in expansion devices and condenser circuiting have significantly reduced cycling losses. Therefore in Figure 4.1 simulation results are shown for a case where C_d ranges from 0.9 to 1.0 ($C_d = 0.9 + 0.1 * \mu$), along with the traditional 0.8-1.0 range used in all other calculations presented here.

The results illustrate how the optimal operating strategies are affected by the magnitude of cycling losses. Instead of over-speeding to 90 Hz as in the base case, it is more efficient to switch to cycling the VS compressor once its speed approaches in the range of 70-75 Hz.

Figure 4.1 also shows the optimal strategy for a 2-compressor system, for both the cases.

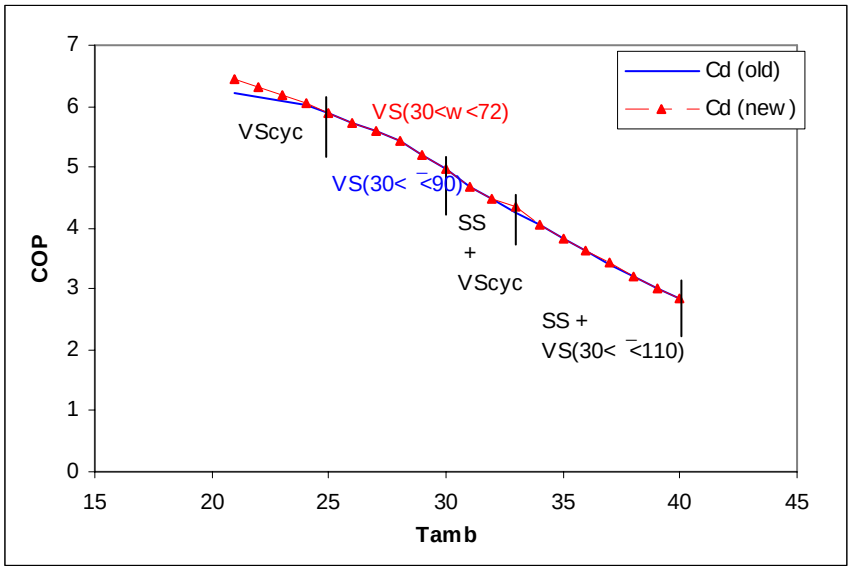

Figure 4.1 Optimal operating strategies for 2 compressor system

The transition points in Figure 4.1 are independent of operating hours, but the overall energy efficiency and optimal Fv will be climate-specific. Using the operating strategy shown in Figure 13 to run the tandem compressors, we can calculate the energy use for any value of F_v. One crude way to identify the optimum value of

Fv, independent of climate and operating hours, is to compare the equally-weighted arithmetic averages of the COP is taken over the entire operating temperature range; the results are shown in Figure 4.2. The optimum value of COP at Fv =0.45 results from the fact that we have to employ the least amount of cycling in this case, and hence the losses are the lowest, hence the COP highest.

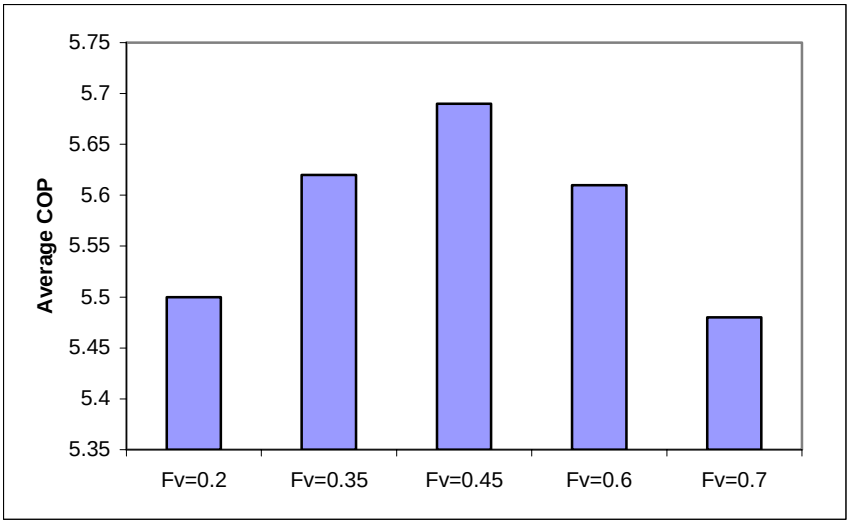

Figure 4.2 COP comparisons between different F_v values

4.2 Optimal strategy for three-compressor system

The next step is to repeat the analysis for a system comprised of three compressors, 1 variable speed and 2 single speed compressors, calculating the system average COP and the load range covered without employing cycling, for different values of F_v.

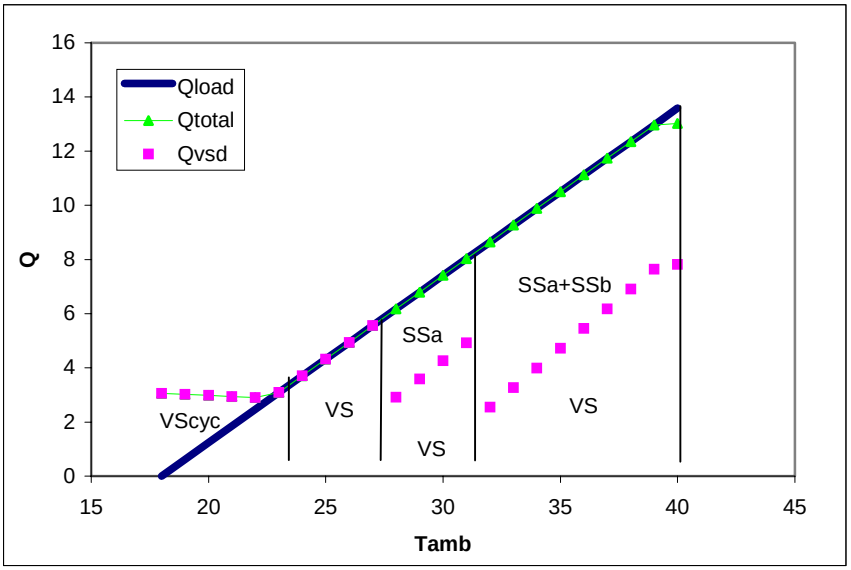

Figure 4.3 Load-capacity for varying T_{amb} curve for F_v=0.45 for the 3 compressor case

The results shown in Figure 4.3 are for the case F_v = 0.45, where the subscripts a and b refer to the two SS compressors, respectively. In the range 18-25°C the VS compressor must be cycled. These results are pretty much

the same that we obtained in case of 2 compressors. However, there is an increase in the value of the system average COP, considering the entire load range for the 3-compressor case, in comparison to the 2-compressor case. This can be attributed to the fact that we now have a higher percentage of time when a more efficient compressor (the SS compressor) is running. The curve shown in Figure 4.3 is plotted assuming that the two SS compressors are equally sized. The size distribution between the two single speed compressors was subsequently analyzed for cases, and the results are plotted in Figure 4.4, which shows us that the case when the SS compressors are equally sized, the system is the most efficient.

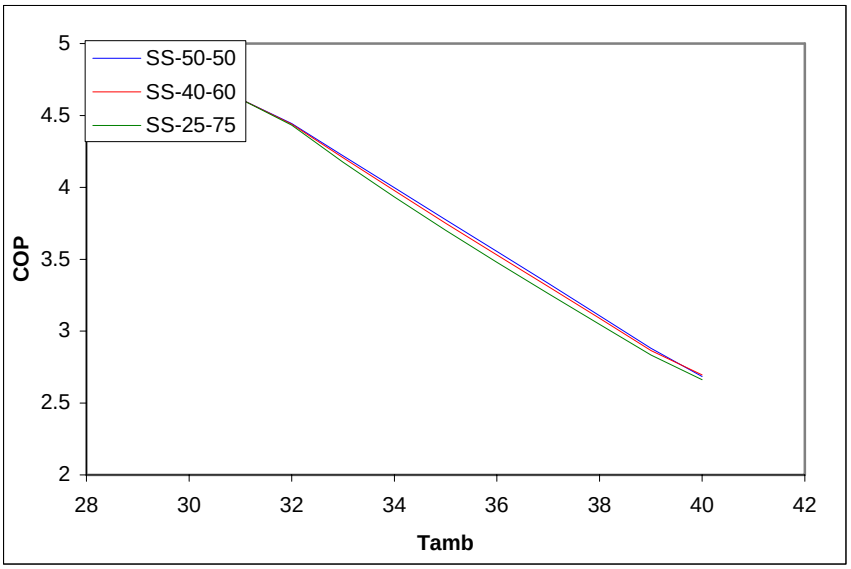

Figure 4.4 COP curves for varying sizing ratios for the SS compressors in the 3 comp system

Proceeding to a similar analysis for the 4-compressor system (1 VS + 3 SS), we observe a slight increase in the average COP value again. However the increase is small and may not offset and oil distribution complexities associated with increasing the number of compressors. In general, through the use of tandem compressors, the average system COP can be increased by as much as 7-9%.

Chapter 5: Seasonal Efficiency Considerations

The above results were obtained assuming that the temperature distribution is horizontal and that each point has an equal weight. However, in real-time situations, the conditions are different, with the temperature distribution being similar to that shown in the Figures 5.1, where we consider the temperature data for a two typical American cities, Pittsburgh and Dallas.

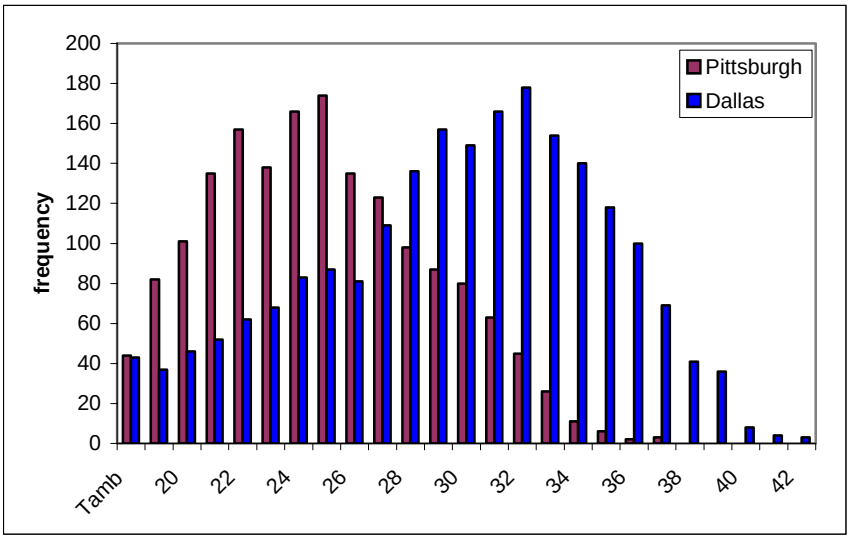

Figure 5.1 Temperature distribution in the cities of Pittsburgh and Dallas

Figure 5.1 shows that distribution of peak cooling loads is different for the two cases, so for the system to be most efficient, we need to choose the values of Fv such that they give the maximum COP in that temperature range. This is shown in the Figure 18, where we plot the COP for different values of F_v. On the basis of the plot, it is seen that the maximum value of COP is obtained at F_v=0.45 for Pittsburgh and at of F_v =0.7 for Dallas. The curve also shows that the COP is fairly insensitive to the value of Fv, and we lose only 3.0% if we choose F_v = 0.45 for Dallas.

In Figure 5.2, the dotted lines show the COP curves using the newer expression for C_d. The optimum values of F_v are almost the same as the previous case, due to the reduced cycling losses, the COP values have increased slightly for all the cases.

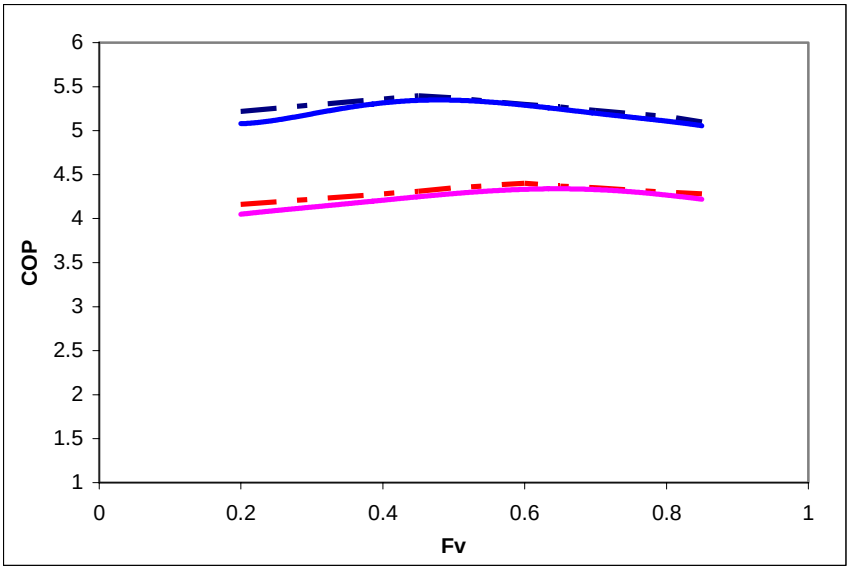

Figure 5.2 Optimum Fv values to meet the loads for Pittsburgh and Dallas

Similarly, compared to the base case with only a single speed compressor, the tandem compressor system increases the COP of the system by around 6.2% for the city of Dallas and around 7.5% for Pittsburgh as shown in Figure 5.3. Compared to a variable speed compressor, the tandem compressor system improves the COP by 2.0% and 2.2% respectively.

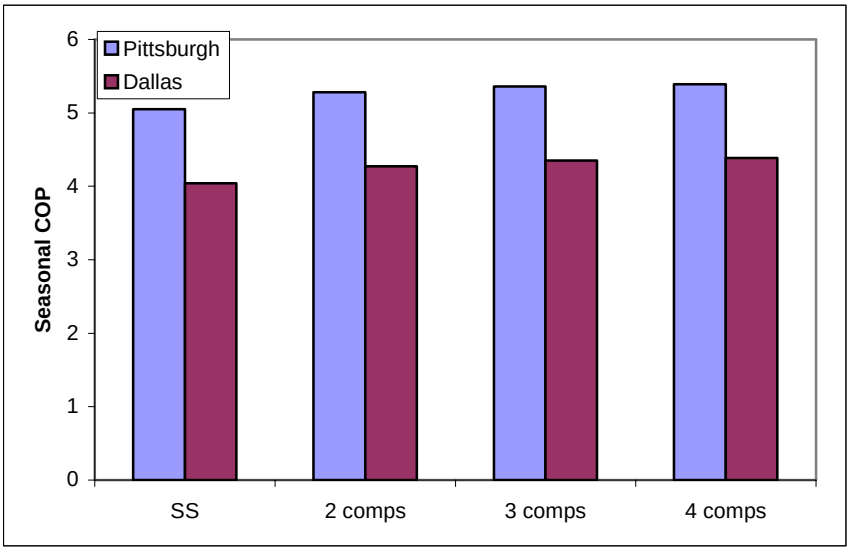

Figure 5.3 Increasing number of compressors increases COP

Chapter 6: Conclusions

From the above analysis, we can hence conclude that using tandem compressors running on an optimum operating strategy helps us in increasing the system COP. The gain is significant over the base (single speed) case, around 7-9%, while compared to the variable speed compressor case we gain around 2.5-4%. The results have been summarized in Figure 6.1, which clearly shows the COP increase obtained with the help of tandem compressors. The plot also points to the fact that increasing the number of compressors helps us in obtaining a further gain in the COP, which is due to the fact that we move towards the more efficient single speed compressor.

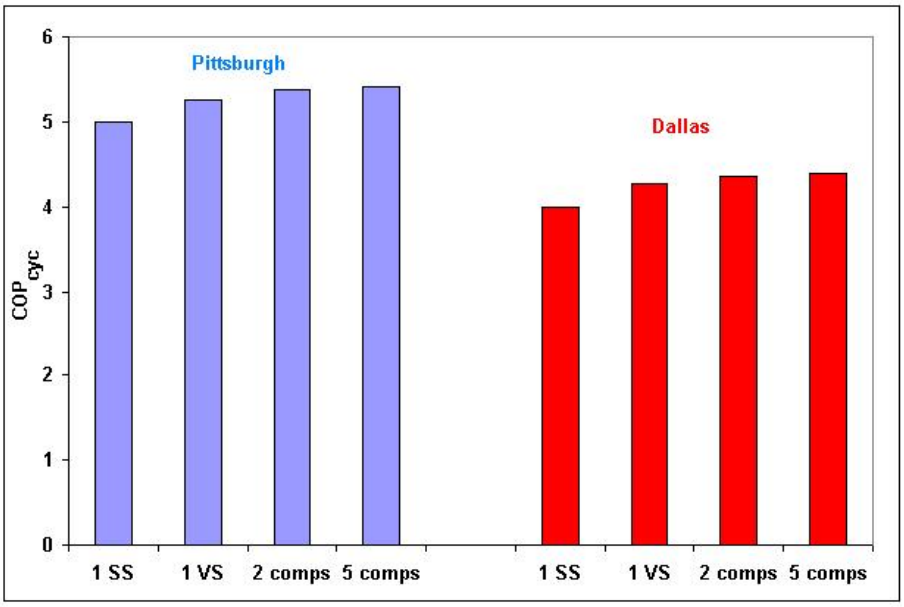

Figure 6.1 Comparison of tandem with base case

Chapter 7: Vapor Injected Scroll Compressors

In the previous section we focused on modulating the mass flow through the system, by distributing the mass between the various compressors, and thus analyzing the effect on the COP of the system. This section focuses on vapor injection, specifically for the case of scroll compressors. Scroll compressors are being widely used in residential a/c and commercial applications. They have lesser efficiency losses due to fewer valves, lower noise levels due to lower pressure gradients and higher motor efficiency due to lower starting needs, as compared to the reciprocating compressors [6]. The refrigerant enters the scrolls at the suction end and through the movement of the scrolls, gets compressed, and is then discharged at the other end. (Figure 7.1)

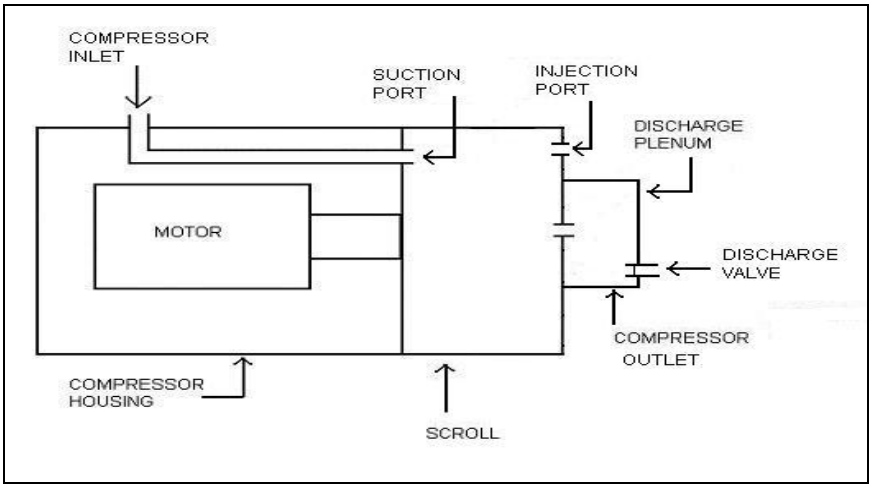

Figure 7.1 Flow of refrigerant inside the scroll compressor

Vapor injection (VI) has been successfully employed in case of the screw compressors, with an increase in both capacity and system COP. Beeton and Pham [7], describe successful implementation of the VI in scroll refrigeration systems using R404A. VI alters the normal refrigeration cycle by adding an injection port to the scroll compressor, as shown in Figure 7.2.

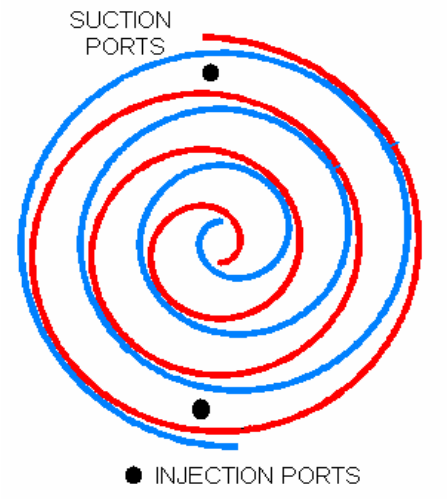

Figure 7.2 Suction and injection ports in a vapor injected scroll compressor

VI divides the compression process in two stages. The mass flow rate at suction at reduced which leads to a reduction in the compressor work, increasing the system efficiency. Similarly, the evaporator quality shifts towards the liquid side, as indicated in Figure 7.3, which results in an increase in the evaporator capacity.

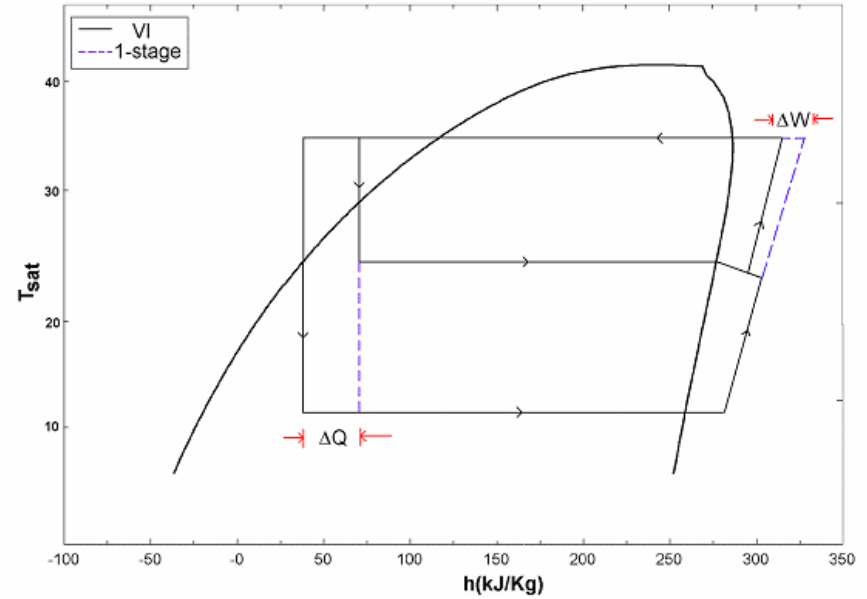

Figure 7.3 Gain in efficiency and capacity using vapor injection

Chapter 8: Ideal Cycle Analysis

Vapor from an internal heat exchanger or a flash tank is injected into the scroll pocket at an intermediate pressure, dividing the cycle into two stages. The refrigerant after passing through the condenser is divided into two parts. The major portion goes through the expansion valve and then to the evaporator, while the remainder passes to the compressor through the injection port. The refrigerant from the evaporator then goes to the compressor where it is compressed in the low stage to an intermediate pressure; then it gets mixed with the injected refrigerant in the scroll pocket. When the refrigerant goes through a second stage of compression and reaches the condenser, the cycle is completed.

One option is to have a Flash Tank after the condenser as shown in Figure 8.1. The entire refrigerant stream is expanded to a two-phase mixture at an intermediate pressure in the flash tank, where the liquid and the vapor phases are separated. The saturated vapor is directed to the injection port of the compressor, while the liquid passes through another expansion valve into the evaporator. The schematic of the cycle is shown as follows.

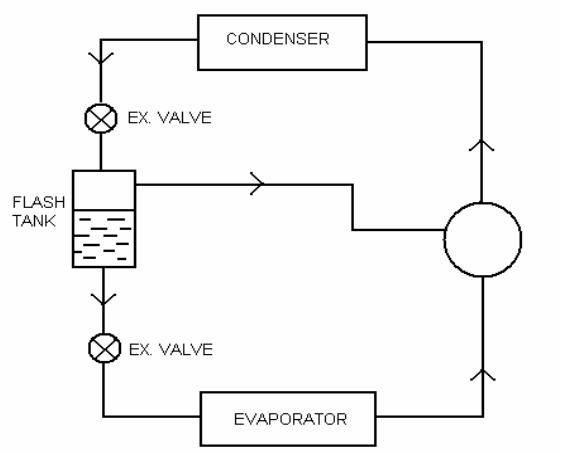

Figure 8.1 Two-stage vapor injection cycle with flash-tank

On the T-h diagram the cycle can be represented as shown in Figure 8.2.

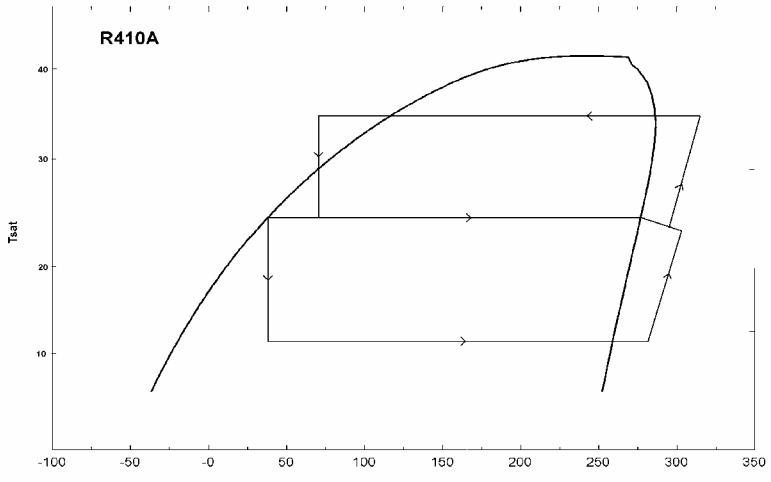

Figure 8.2 T-h diagram of vapor injection cycle with flash-tank

The mass and energy balance equations at the point of mixing are:

$$m_{HPin} = m_{LPout} + m_{inj}$$

$$m_{LPout} * h_{LPout} + m_{inj} * h_{inj} = m_{HPin} * h_{HPin}$$

A second option shown in Figures 8.3 and 8.4 uses a heat exchanger in place of the flash tank. A certain amount of refrigerant is bled off just after coming out of the condenser and is expanded to the intermediate injection pressure and leaves the counterflow internal heat exchanger in the saturated vapor state after subcooling the remaining liquid refrigerant, which proceeds through the expansion valve and into the evaporator.

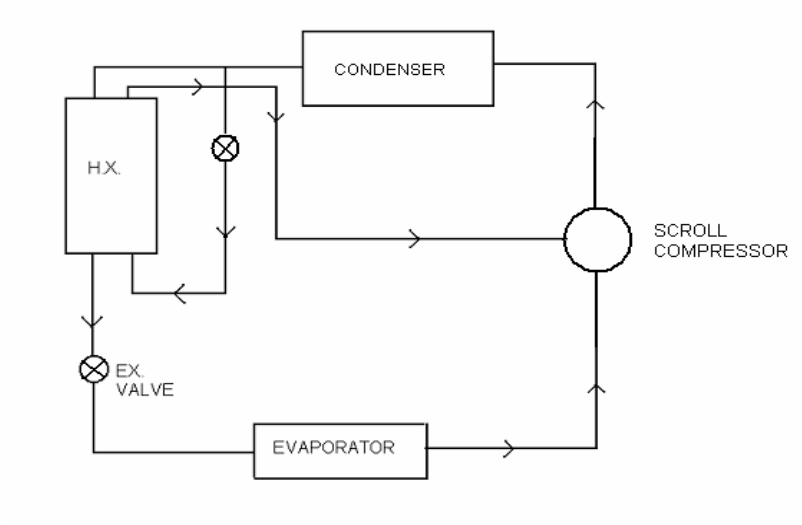

Figure 8.3 Two-stage vapor injection cycle with heat-exchanger

On the T-h diagram, the cycle can be represented as:

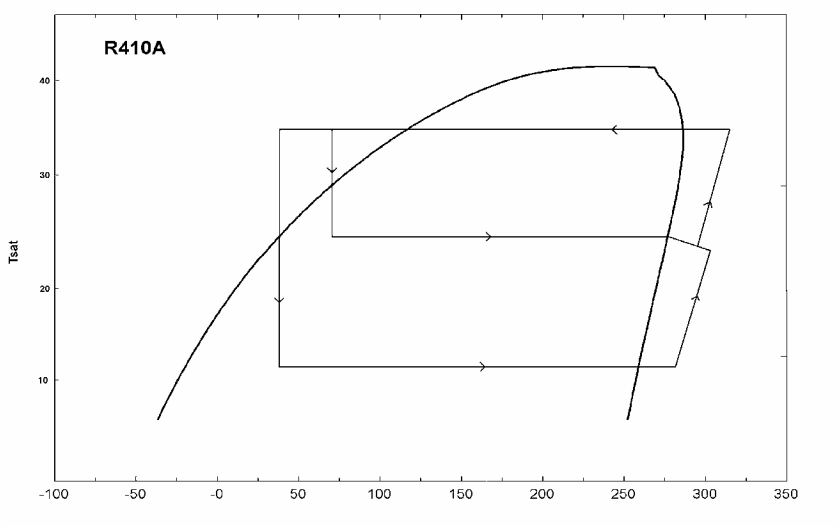

Figure 8.4 T-h diagram of vapor injection cycle with heat-exchanger

A simple ideal gas analysis of an isentropic two-stage compression process predicts that the minimum work done (or maximum COP) is obtained in a case when the intermediate pressure is equal to the geometric mean of the condenser and the evaporator pressures. For our simple model, we assume that the compressor has a constant

isentropic efficiency (=0.7), and the cycle has an ideal HX (100% effectiveness), or an ideal FT, (one which injects the vapor at an exit quality of 1). It is also assumed that there is no superheating in the evaporator or sub-cooling in the condenser. (See Appendix B)

Next, we try to identify the location of the injection port that would lead to the optimum COP, by doing a parametric analysis for different values of injection pressure. From Figure 8.5, it is evident that for the ideal cycle, the maximum COP is obtained at a $P_{inj} = sqrt(P_{cond}*P_{evap})$.

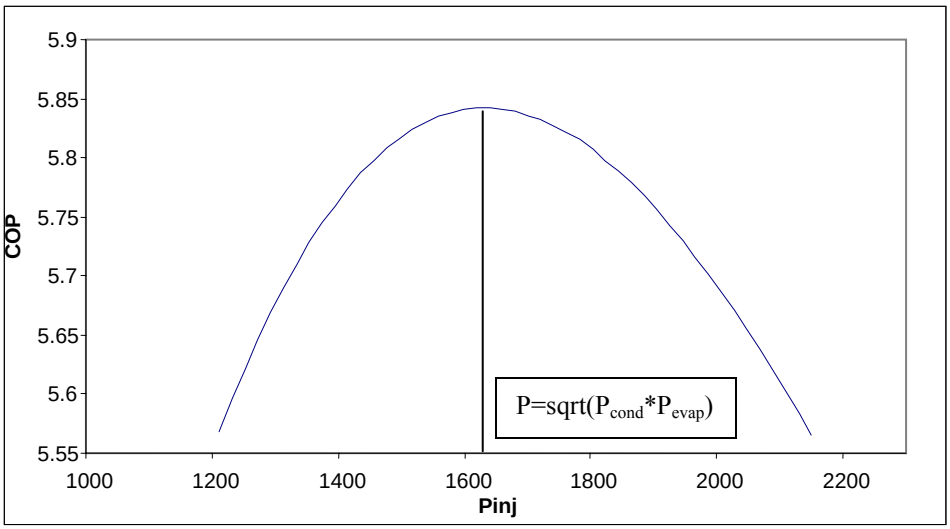

Figure 8.5 COP curve as a function of injected pressure for an ideal FT or HX model for ARI-A conditions

Using a simple cycle model and comparing the results to an ideal cycle without injection, and sizing the two systems so that they meet the same load at a given design condition, it is observed that the COP of the VI case is higher than the base case by almost 8%.

The analysis is then extended to real systems, followed by a parametric analysis to access the benefits of vapor injection for both air-conditioning and refrigeration applications over a whole range of operating temperatures.

Chapter 9: The Vapor Injection Cycle (Real System)

For an ideal HX, we need to have an infinite area, which is not possible in real systems. Similarly it is very hard to prevent some droplets from leaving the flash tank along with the vapor, as is specified by an ideal FT. Hence we model each component of a real system individually, and then model them together.

The most important part of this cycle is the compression process, due to the presence of the scroll compressor. Compression within the scroll takes place through the movement of the trapped pocket within the scrolls while the volume is decreasing. For the modeling of the real systems, we first need to understand the compression process.

9.1 Compression process

The compression process, taking place inside the scroll compression can be described as follows. The suction gas passes through the housing and into the chamber around the compressor mechanism and motor, filling the cavity with low-pressure gas at suction conditions. After cooling the motor, the gas is then drawn into the suction inlet of the scroll set and compressed between the wraps, after which it passes through the discharge port and into a discharge plenum above the fixed scroll. This plenum is connected in turn to the discharge tube through which the gas exits the housing and passes into the system. A check valve present at the exit of the compressor prevents the back-flow of the refrigerant from the condenser.

9.2 Under- or over-compression

Scroll compressors have a fixed internal volume ratio, defined by its geometry, and selected for a given design condition. After entering the orbiting scroll, the suction gas gets compressed by this ratio. Unlike reciprocating and rotary compressors that have a discharge valve to exhaust the compressed gas only when the cylinder pressure reaches the high side pressure, the scroll wraps will compress the gas to the design volume ratio regardless of the operating pressures. Only when the discharge pressure is at the design compression ratio will optimum compression efficiency be achieved.

If the operating pressure ratio is lower than the design pressure ratio, the gas is over-compressed, increasing power consumption and reducing efficiency. The over-compressed refrigerant is discharged into the discharge plenum, and expands isenthalpically to the condenser pressure as shown in the Figure 9.1.

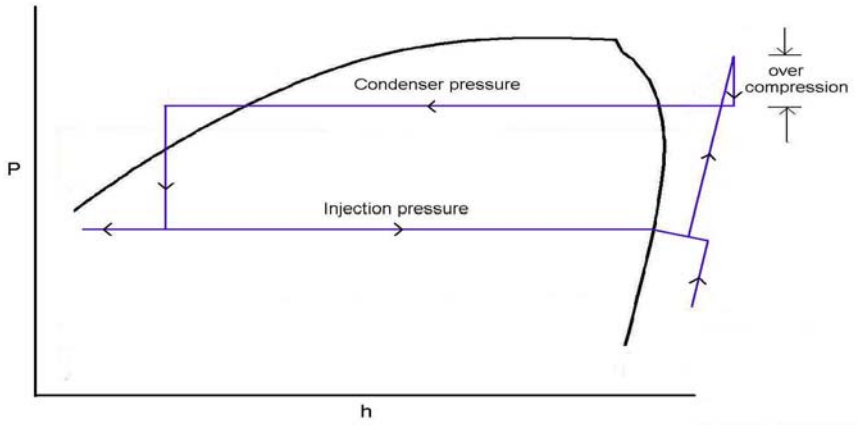

Figure 9.1 Over-compression in the scroll compressor

Similarly, if the operating condition pressure ratio is higher than the design compression ratio, the refrigerant is under-compressed. More compressor work has to be done to get it to the discharge pressure, thus lowering the overall compressor efficiency as shown in Figure 9.2.

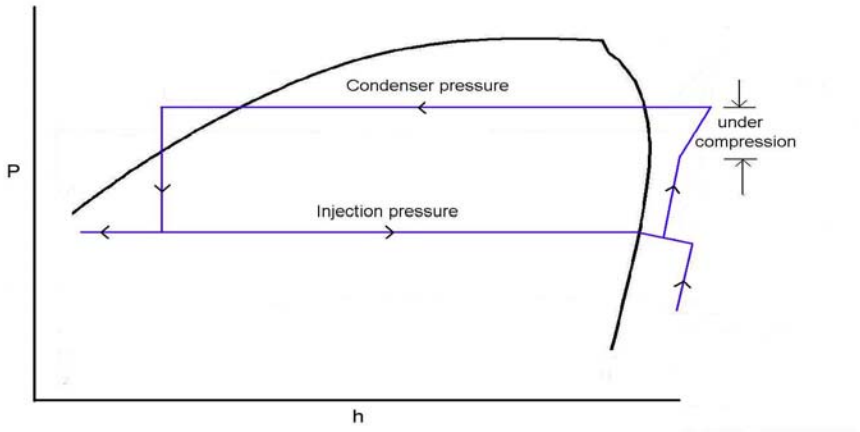

Figure 9.2 Under-compression in the scroll compressor

9.3 Work required for over- and under-compression

For majority of the time, the system is operating at non-design conditions, and thus both over and under compression occurs, resulting in a loss in the system efficiency. During over-compression, the refrigerant is compressed more than it is required, and the extra work is dissipated as the refrigerant expands isenthalpically to the condenser pressure and the system COP decreases.

During under-compression, the refrigerant leaves the scrolls at a pressure less than the condenser pressure, and cannot flow into the condenser. The check valve at the exit of the discharge plenum prevents back-flow of high-pressure refrigerant from the condenser into the discharge plenum. The refrigerant coming out from the scroll fills into the discharge plenum. More mass keeps on adding to this mass until the pressure in the discharge plenum is equivalent to the condenser pressure. As soon as it exceeds this value, the check valve opens and the refrigerant flows into the condenser.

This process can be simulated as a tank-filling problem, with a valve at one end. There is some refrigerant in the plenum, at the pressure discharged by the scrolls. By adding more mass to it, the pressure rises high enough, so that it matches the condenser pressure, and refrigerant flows to the condenser through the discharge valve as shown in Figure 9.3.

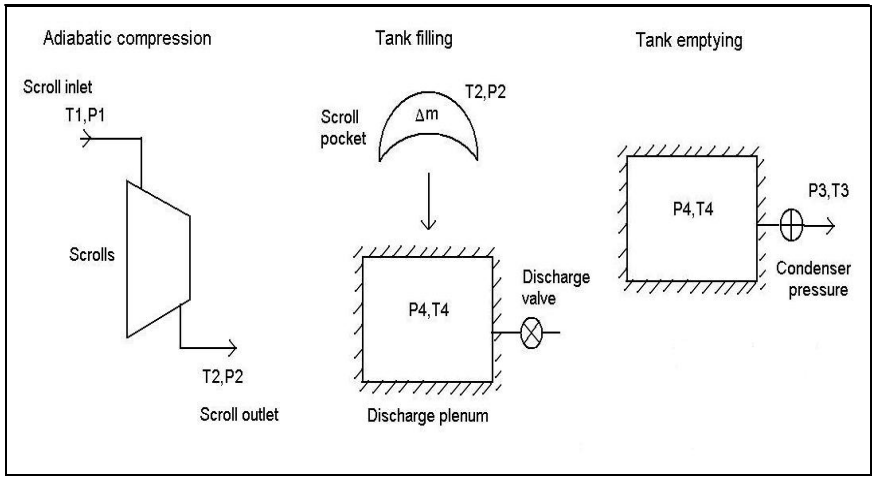

Figure 9.3 Schematic of the under-compression process

By allowing an extra amount of mass to flow into the plenum, the pressure rises from P2 to P4, which we assume is slightly higher than P3. The work involved with this process is given by the following expression.

$$\text{Work} = (m+\Delta m)*u_4 - m*u_3 - \Delta m*h_2$$

Similarly, for the tank emptying process, the work associated, using the first law energy balance can be given by the expression.

$$\text{Work} = m*u_3 - (m+\Delta m)*u_4 + \Delta m*h_3$$

Adding the work associated with these two processes, we get,

$$\text{Total Work} = \Delta m*(h_3 - h_2)$$

However, this would be the case if we assume the processes to be isentropic in nature. For a real system, we have to take an isentropic efficiency term into account. We get the expression for this efficiency from the compressor data. Hence the work is calculated as given by the following expression.

$$\text{Total Work} = \Delta m * (h_3 - h_2) / \eta_{isen}$$

9.4 Validating the over/under-compression model

We check the validity of the above assumption by comparing the results obtained from the simulation model to the compressor calorimeter data provided by the manufacturer [8]. With R410A as the refrigerant, the isentropic efficiency was calculated at each of the 24 calorimeter test points.

At one of the calorimeter test conditions, the volume ratio during the compression process equals the in-built ratio of the scrolls, and the isentropic efficiency was found to be 0.69 at that condition. At all other operating conditions, the scrolls compress the fluid by the same ratio, so it is assumed that the isentropic efficiency of that part of the process would be the same. The additional work due to over/under-compression is then added, and the total compared to the data in Figure 9.4. Since the agreement is satisfactory, the same approach is employed in simulating the multistage compression process of the vapor-injected compressor.

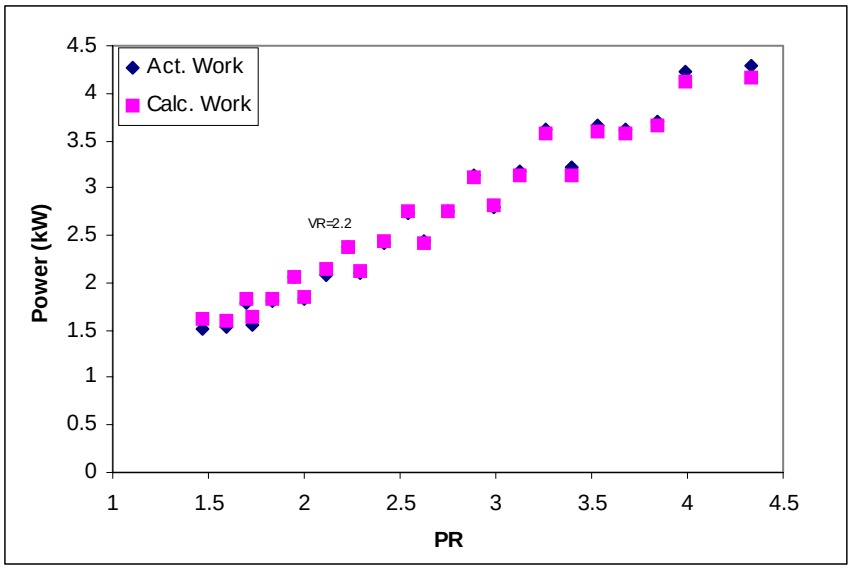

Figure 9.4 Comparison of model results with experimental data

9.5 Pressure drop at injection point

Another point of interest in case of the real system is the modeling of the injection port. The refrigerant entering through the injection port must be at a pressure higher than that of the refrigerant discharged from the LP stage of the compressor. This difference in pressure ensures the refrigerant coming from the flash tank or heat exchanger gets injected into the scroll pocket passing the injection port. The following calculation shows that the pressure difference can be made negligibly small through appropriate choice of a few key design parameters. To estimate the required pressure difference, we assume that the port diameter (D_{port}) is 6 mm and the orifice factor (C_D) is 0.9. Also,

$$\Delta m = m_{Inj} * \Delta t$$

$$\Delta m = f(\Delta p, C_d, D_{port})$$

We assume arbitrarily that the injection port is open for $1/10^{th}$ of the revolution. Calculations show that the value of this pressure difference is fairly small, of the order of 10 kPa. Increasing Δt to $3/10^{th}$ of revolution reduces this value to around 4-5 kPa. Since the value of this pressure difference is very small compared to the operating pressures, the effect on the cycle is quite small and can be neglected in the following analyses.

Chapter 10: Air-Conditioning Applications

We start by considering the air-conditioning cycle, assuming R410A to be the refrigerant. For the HX model we assume that the mass flow of injected vapor is regulated to produce 5°C superheat at the injection point, and that for the FT model, there is no superheat.

Instead of modeling a condenser of a particular geometry, it is assumed that the condenser's entering temperature difference is 10°C at the ARI-A design condition, and varies linearly with ambient temperature.

$$T_{CDin} = T_{amb} + 10 * (Q_{cond} / (W_{total} + (Q_{load})_{des}))$$

or,

$$T_{CDin} = T_{amb} + 10 * ((W_{total} + Q_{evap}) / (W_{total} + 10.5))$$

Q_{cond} is the condenser heat rejection and Q_{evap} is the evaporator capacity. Q_{load} is assumed to vary linearly with ambient temperature from zero at an ambient temperature of 18°C, to 10.5 kW at the design outdoor temperature of 35°C. For an actual building, loads will vary around this line due to radiative gains through windows, and due to latent and internal loads, but for purposes of this analysis, the equation can be taken to represent the mean at any ambient temperature.

$$Q_{load} = (10.5 / (35 - 18)) * (T_{amb} - 18)$$

For the evaporator we choose the geometry in a manner such that, at the design point, the T_{evap} is 12°C. The UA value for the evaporator is calculated as 1.625. The value is then fixed for both the VI and the base case, and serves as a representation of the evaporator geometry. Using these assumptions, we develop our real model and then proceed further.

10.1 Locating the vapor injection port

We have to determine the point where the refrigerant is to be injected to ensure that we achieve the maximum system COP. This COP shall be maximized for operating condition ARI-B (T_{amb}=28°C), after the compressor has been sized to meet the load of 10.5 kW when the ambient conditions are at 35°C. The results for the real HX case are shown below in Figure 10.1. For the ideal FT or HX, the maximum COP is obtained for at a VR of 1.4. However, in our model, due to the subcooling and superheating effects, as well as the non-isentropic compression processes, we get the maximum COP at a volume ratio 4% higher to the ideal case Here a real HX of effectiveness 0.9 is considered (equivalent to an real FT, where the injected vapor is at x=0.96 quality).

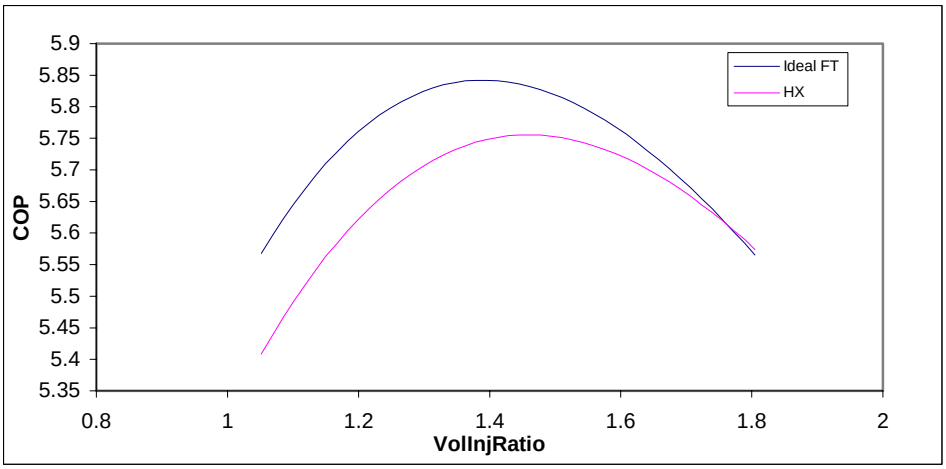

Figure 10.1 COP-Volume injection ratio curves for the ideal and real HX case.

As the ambient temperature varies, so would the optimal injection pressure. Figure 12 shows the locus of the optimal injection saturation temperatures over the typical operating range. It seems that with the rise in the ambient temperature, the $T_{sat,inj}$ leading to optimal COP rises linearly. In a real system the location (volume ratio) of the injection port is fixed at the volume ratio that maximizes COP at the ARI-B condition (28°C outdoor). The implications of optimizing its location for other ambient temperatures are shown in Figure 10.2.

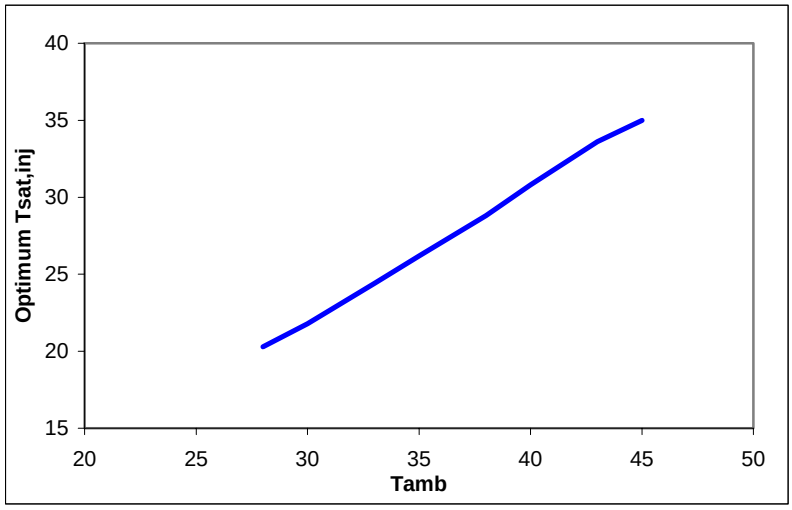

Figure 10.2 $T_{sat,inj}$ for maximum COP, as a function of varying ambient temperature.

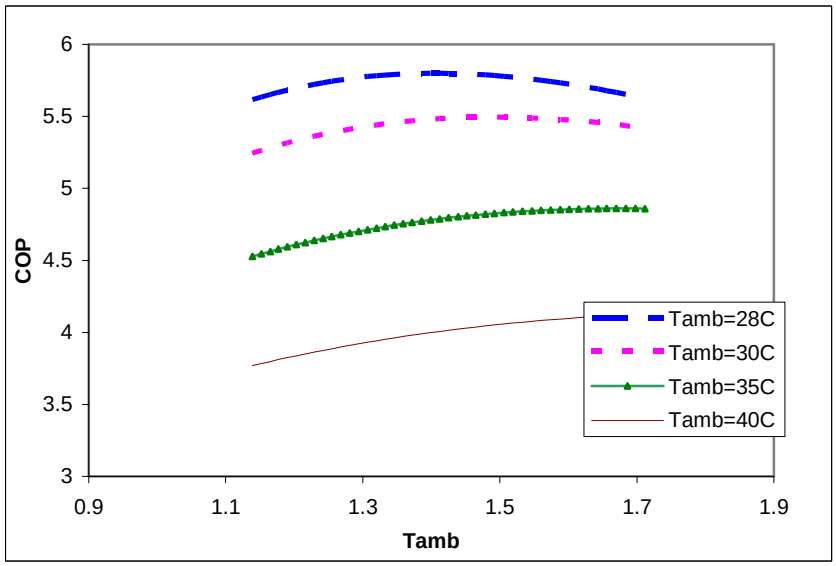

Figure 10.3 COP as a function of Intermediate pressure at various ambient temperatures

By fixing the injection port location at volume ratio 1.4, we observe that we incur a COP penalty ranging from 0.3% at T_{amb} = 30C, and 4% at T_{amb} = 40°C, relative to a hypothetical ideal case in which the location of the injection point could be varied continuously.

10.2 Capacity calculations

For the real system, we assume the VI system with a HX of 90% effectiveness. The model is next analyzed for an entire range of operating temperatures, and the results are compared with the base case. We size both the models such that they are able to meet a load of 10.5 kW (=3 tons) at the ARI-A (Tamb = 35°C), and then compare the capacity of the system over typical ambient temperature range (20-35°C) for air-conditioning applications. Figure 10.4 compares the VI scroll compressor cycle with the base case of no injection.

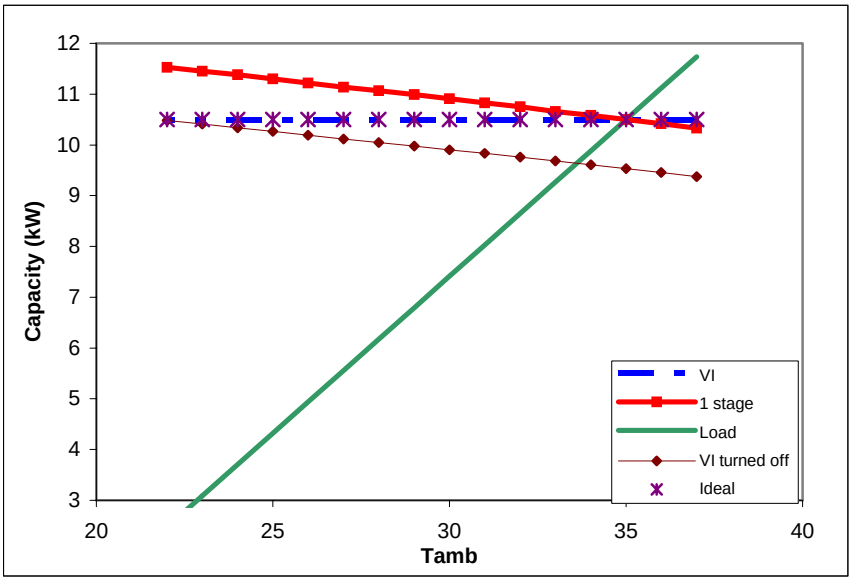

Figure 10.4 Capacity comparison for the cases with and without vapor injection.

Notice that in the base case, with the drop in ambient temperature, there is an increase in the capacity. For the ideal VI system, the capacity remains constant. The real VI system capacity deviates only slightly from the ideal. The net effect of this behavior is to help reduce the run time fractions. The line lying below and parallel to the single stage case represents the capacity of a system, having a compressor sized as in the VI case, but operating with VI turned off. It is clear that VI is not needed to meet the load except when the ambient temperature exceeds 33.2°C, and that its cycling losses will be smaller on all cooler days. However shutting off VI foregoes the benefit of the more efficient 2-stage thermodynamic cycle, so the optimal operating strategy at any temperature will depend on the relative magnitudes of these two offsetting effects.

From Figure 10.5, we see that the run-time fraction for the VI case is higher than then base case by around ~5-7% in the given temperature range, which means that we shall have lower cycling losses. The cycling losses are negligible while we are operating close to the design condition, but increase up to around 8-10% of the COP value for ambient temperature conditions 12-15°C away from the design condition.

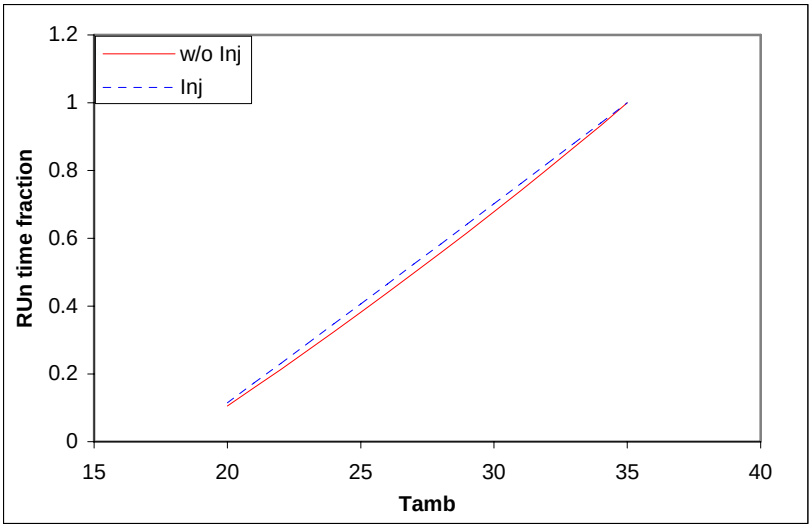

Figure 10.5 Run-time fractions for the cases with and without vapor injection.

From Figure 10.4 we notice that for the VI case, the capacity of the system, tends to remain almost constant emphasizing the fact that the VI system is fairly insensitive to ambient temperature. This can be explained on the basis of the following t-h diagram (Figure 10.6).

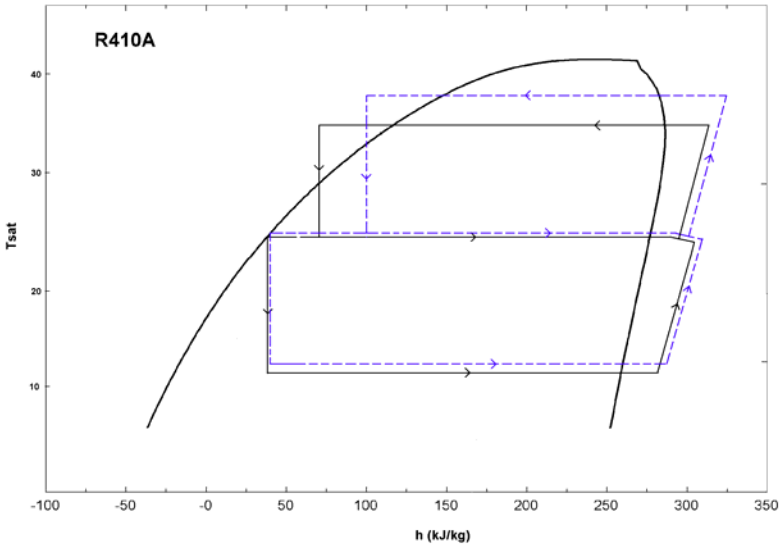

Figure 10.6 t-h diagram of VI system with flash tank

The solid lines indicate the cycle for a given ambient temperature condition. The dashed lines refer to the cycle at an ambient temperature higher than the previous case. The condenser temperature increases in accordance with the ambient temperature. Since only the liquid portion enters the evaporator, the points on the lower half of the cycle remain more or less the same. Also, the mass flow rate through the evaporator remains almost constant, since with the changes in the ambient, the fraction of injected mass changes, and it affects only the top half of the cycle. Therefore, as we have almost the same mass flow rate, and roughly the same T_{evap}, the capacity of the system, remains unaffected by the changes in T_{amb}.

However, for the base case, with the change in the T_{amb}, all the points in the cycle shift. Also, the mass flow rate changes, and the T_{evap} changes considerably, hence the capacity of the system changes automatically, as can be seen from Figure 10.7.

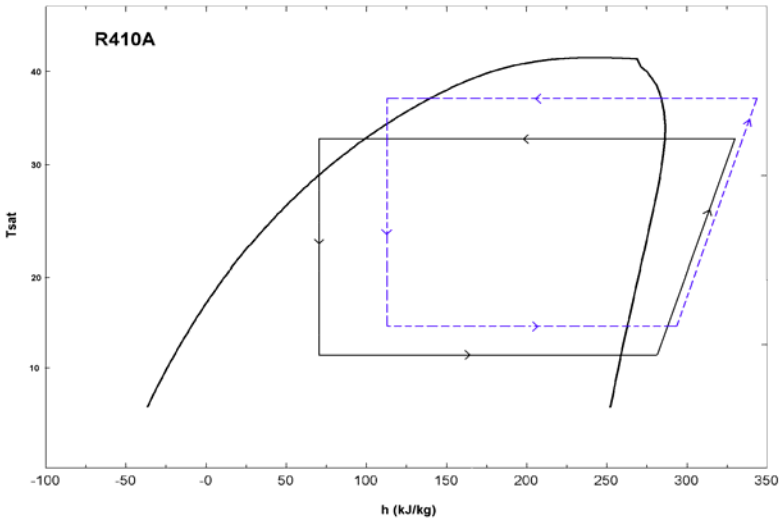

Figure 10.7 T-h diagram of simple air-conditioning cycle

10.3 COP comparisons

As suggested by the ideal cycle, VI helps increase the COP of the system. Figure 10.5 suggests that the compressor needs to be cycled to match the load at any operating condition other than the design condition, so the cycling losses are approximated by a multiplicative factor C_d applied to the COP term. As defined by the ARI standards [4], an expression for this factor is given as follows.

$$C_d = 0.8 + 0.2 * \mu$$

μ in the above equation is the run-time fraction. Taking into account this factor, we next compare the COP values between the VI and the base case.

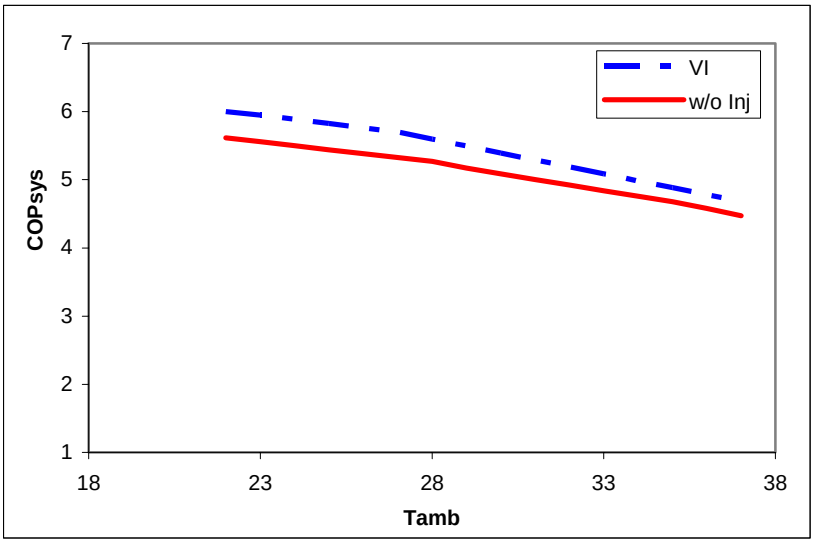

Figure 10.8 Cycle COP comparison between VI and base case.

From the plot, we notice that the COP of the VI scroll compressor cycle is around 6-8% higher than the compressor cycle without injection, in the ambient temperature range of 22-37°C.

Also, we notice that there is a point (at T_{amb} = 27°C) for both the curves, This point marks the boundary between over and under compression. Theoretically, the slope of the COP curves would increase at low T_{amb}, because of the reduction in the temperature lift. However, the extra work associated with overcompression overwhelms this effect, and thus shows up as a decline in the slope. Because of the more pronounced effects of over-compression, scroll compressors are designed with a value of volume ratio, which generally restricts over-compression to some limited cases. (Appendix C)

10.4 Compressor sizing

Figure 10.9 explains why the VI cycle requires a compressor 16% smaller than the base case with no injection. Notice that for the same operating conditions, the enthalpy change across the evaporator is higher for the VI case than the case when there is no injection. This would mean that for the same conditions, to achieve the same capacity the VI system would require lesser mass flow rate, or eventually a smaller compressor size.

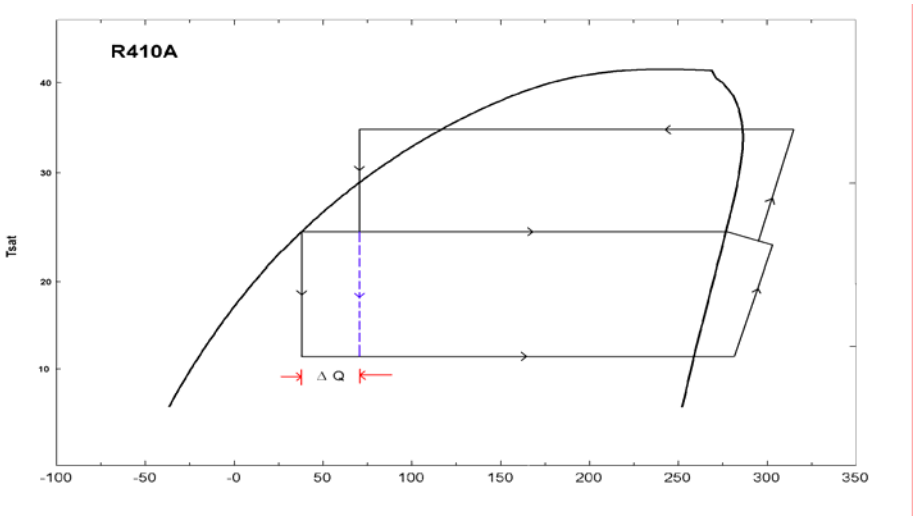

Figure 10.9 T-h diagram for the VI-scroll cycle

10.5 Capacity modulation

Another advantage sometimes cited for VI scroll compressor systems is its ability to provide capacity modulation. It is true that vapor injection increases the capacity of a given compressor. This benefit is captured by using a smaller compressor to meet a given design load. Actually the potential for capacity modulation is quite limited, and can be achieved by either using a solenoid valve or by throttling the injected vapor.

The solenoid valve provides a binary means of modulating capacity. When the ambient temperature drops, we can switch the solenoid valve off to stop injection, thus reducing the capacity of the system but sacrificing the efficiency benefits of vapor injection. At higher ambient temperatures temperature, the solenoid valve can be switched back on to meet the load. This method can however, only provide us with two capacity points, one with the valve on and the other with the valve off. Unless the cycling losses were very large, this would not be an effective strategy.

Another way of modulating capacity would be by throttling the injected vapor. The vapor can be throttled using the TXV to modulate the degree of superheat of the injected vapor, for example by increasing it from 5°C to 15°C. However, using this method has negligible effect on the capacity of the system; it increases by only about 0.7%.

10.6 Combining vapor injection with variable speed drive

The run-time fractions obtained for the VI case go down fairly low values (~0.15) which means that cycling would have to be employed for a significant part of the operation time, and in turn leading to cycling losses. One method of reducing these losses would be through the use of a variable speed compressor. Variable speed drives can improve cycle efficiency by reducing condensing temperatures and avoiding cycling losses. This section explores the possibility of combining this option with vapor injection. The variable speed drive has some inverter losses (~4%) associated with it. For this example, we assume that the compressor can be operated in a speed range of 30 to 110 Hz. Over this speed range the isentropic efficiency varies as a quadratic function of speed [9], and this fact has been taken into account by normalizing the efficiency term for a speed of 60 Hz, and is represented by the following equation.

$$\eta_{speed\,/\,60} = -0.08 * (\omega/\omega_{60})^2 + 0.1411 * (\omega/\omega_{60}) + 0.9337$$

We compare these results with the base case, with no injection, and the results are shown in the Figure 10.10.

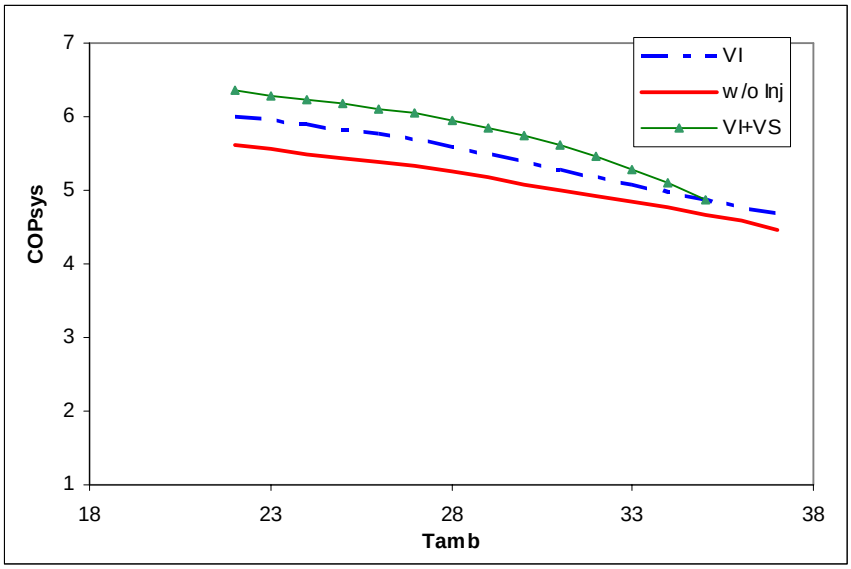

Figure 10.10 COP comparisons for single and variable speed cases.

From the plot we notice that at the design point (T_{amb}=35°C), the variable speed (VS) COP is less than that of the single speed injection case. This is because of the losses in the inverter drive (~4%), and due to the lower isentropic efficiency of the compressor when it is running at its 110 Hz maximum speed. However, the VS system has a higher COP at almost all the ambient temperatures. This is due to the fact, that with the modulation in speed the mass flow rate changes and it reduces the work done by the compressor.

Also we notice a point of inflection for all the plots. Towards the left of this point, all the curves show a drop in the value of COP. This is the point where over-compression starts and thus the COP drops. There are two points of inflection on the variable speed curve. The first point (T_{amb}=28°C) denotes the start of cycling, and the associated losses show up with a reduction in the slope of the curve. The second point (T_{amb}=23°C) indicates the start of over-compression, and the effects of the over-compression losses can be seen in the form of a drop in the subsequent COP values.

Similarly in Figure 10.11, we have the plots of the run-time fractions for the variable speed cases versus the base case. The fractions for the VS option are much higher (~40-60%) than the single speed case and thus have lower cycling losses (12-15%) as compared to the single speed case. The flattening of the capacity curve (Fig. 10.4) accounts for the higher runtime fraction with VI.

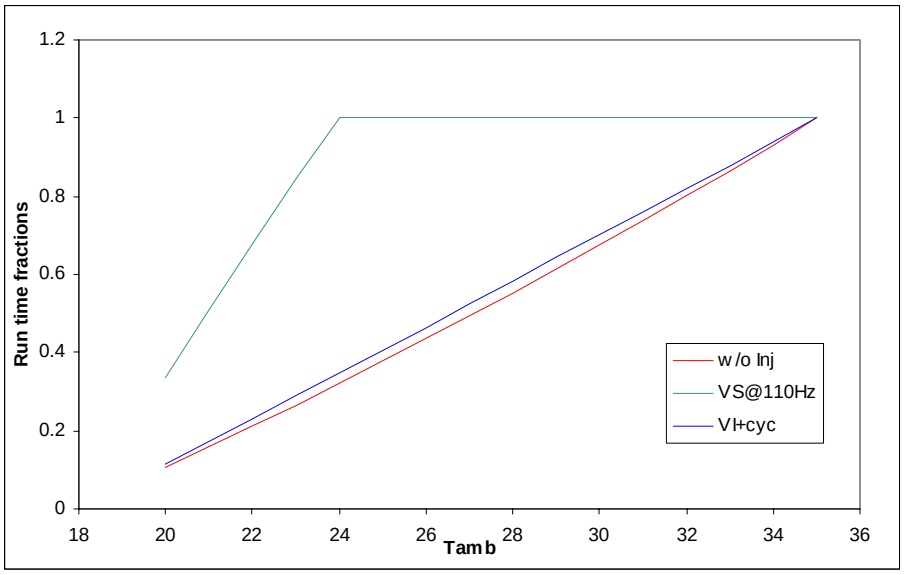

Figure 10.11 COP comparisons for single and variable speed cases.

Chapter 11: Refrigeration Applications

One major difference between the air-conditioning and refrigeration compressor is the presence of a dynamic valve between the exit from the scrolls and the discharge plenum, in the latter, which prevents over-compression. Hence, we do not employ the same approach that we had adopted for the a/c model. In this case, the dynamic valve opens as soon as the refrigerant reaches the condenser pressure. Thus it lets the refrigerant to be compressed to different volume ratios, depending on the operating conditions. Since we would now be working in a higher temperature lift, we choose a compressor with a higher volume ratio. For the refrigeration applications the Copeland ZF18K4KE scroll compressor is taken which has a VR = 2.93. From the compressor data, it is found that the isentropic efficiency varies as a linear function of the pressure ratio, and is given as follows.

$$\eta_{isen} = 0.856 - 0.0487 * (PR)$$

Using the above expression, the model is then analyzed for the refrigeration applications. The return gas is assumed to be at 18.33°C (65°F). Both the VI and the base case are sized so that at the ARI-A conditions the evaporator temperature is -10°C, and the load on the system to be a constant value of 10kW.

A similar analysis, as we did for the previous case, thus choosing a suitable injection point for that same -10°C operating condition. Once, we have decided on the location of the port, we go on to compare the results with the base case. The COP comparisons are shown in Figure 11.1.

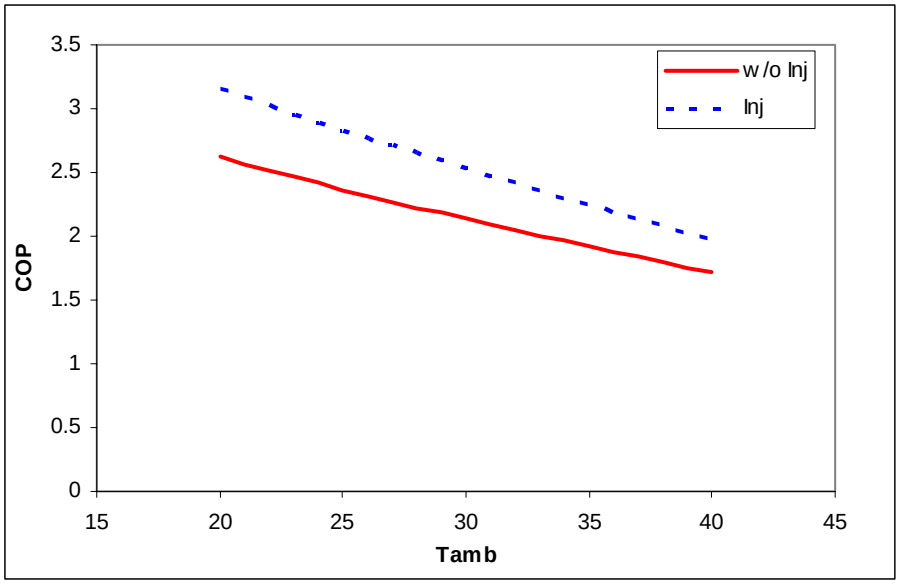

Figure 11.1 Efficiency effects of vapor injection in refrigeration applications

We see that the COP of the system increases significantly for the case when we use the VI scroll compressor cycle. The COP increases as much as 15% in the temperature range of 20-40°C. This could be attributed to the fact that we are now working in a larger temperature lift between the evaporator and the condenser temperature, as compared to the air-conditioning case. Another noticeable fact is that the slope of the VI curve is increasing as the temperature falls. As the temperature falls, the run time fractions fall along with it. For the VI case, the run-time fractions are greater than in the base case, and the reduction in cycling losses is apparent.

Similarly, Figure 11.2 shows that the VI cycle increases runtime fractions around 4-7%, which would result in 3-4% lower cycling losses.

As the values of the run-time fractions are fairly high for the entire operating range (0.91~0.99), we do not install a variable speed drive for the refrigeration case, as it would not provide any added benefit.

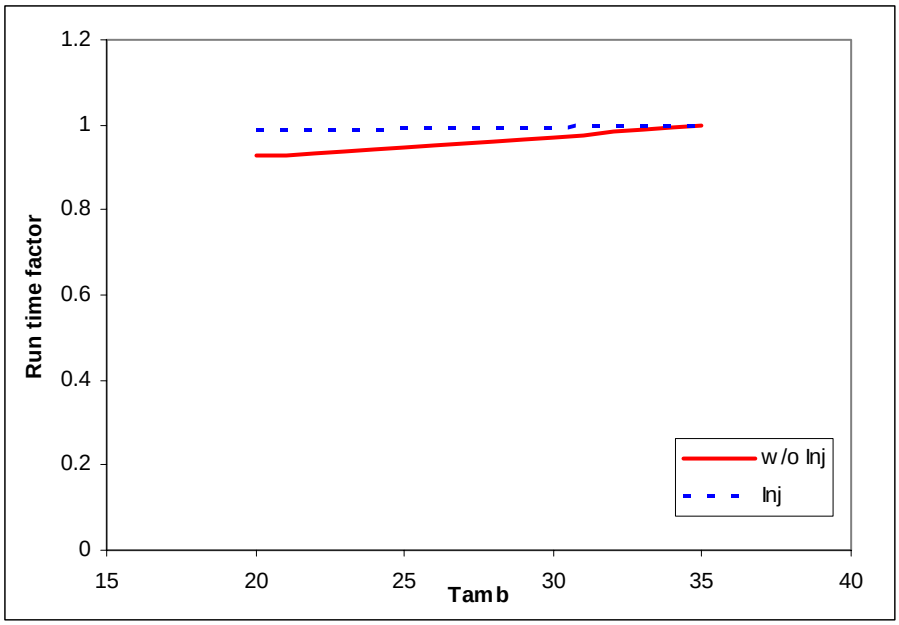

Figure 11.2 Run-time fraction comparison for refrigeration

A significant factor is the compressor size. With the help of vapor injection in case of refrigeration applications, the size of the compressor can be reduced by as much as 30% than the base case, to handle the equivalent load at the 35°C outdoor ambient design condition.

Chapter 12: Conclusions

On the basis of the above analysis we conclude that vapor injection at the compressor has two major effects on the system. The first is a cycle efficiency increase; the second is that vapor injection enables use of a smaller compressor displacement to provide a given system capacity. However, the motor must be sized for the maximum capacity, with or without vapor injection.

A third, but smaller, effect was also quantified. The vapor injection cycle's capacity remains almost constant as ambient temperature and load decreases, thus reducing cycling losses by increasing runtime fractions.

VI should not be viewed as a capacity modulation technique. Varying the injected mass flow at a fixed volume ratio will reduce the compressor mass flow rate, but at the cost of the efficiency gains associated with the vapor injection cycle. A cursory analysis quantified the potential benefits from employing vapor injection in a variable-speed compressor. The results are as follows:

- COP improves by ~8-10 % for a/c applications and by ~15% for refrigeration applications.
- Cycling losses reduced by around 8-9% for a/c applications and 4-5% for refrigeration applications. Stated another way, cycling loss reductions account for around 2% of the 6-8% savings in a/c and about 0.8% of the 15% savings in refrigeration energy.
- Size of the compressor reduced by 16% for a/c applications and by almost 28% for refrigeration applications.
- Adding a variable speed drive to the vapor injected cycle in a/c applications can increase the COP by an additional 10-12% at part load conditions.

The above results were obtained assuming a cycling degradation coefficient of 0.8-1.0. However for modern, more efficient systems, cycling losses are only half as large, so part-load efficiency improvements attributable to vapor injection would be reduced accordingly. Most of the efficiency improvements result from improving the cycle – short-circuiting a fraction of the refrigerant so it needs to be compressed by a lesser amount.

The results show that VI technology offers significant advantages in applications where temperature lift is high (e.g. water heating, space heating and refrigeration), and relatively smaller benefits in applications such as residential a/c where efficiency standards are based on tests conducted at very low temperature lift conditions. This could explain why VI technology is more widely known and used in residential applications in Europe and Asia, compared to the US where the residential market is focused almost exclusively on air conditioning applications.

References

[1] Muir, E.B., private communication regarding efficiency of ZP32K3E-PFV compressor, *Copeland Corporation*, Sidney OH, November 2002.

[2] Park Y.C., private communication regarding the speed characteristics of the variable speed compressors. October 2002

[3] Park Y.C., Kim Y. and Cho H., Thermodynamic analysis on the performance of a variable speed scroll compressor with refrigerant injection, *Intl. Journal of Refrigeration* Volume 25, December 2002.

[4] Air-conditioning and Refrigeration Institute, Unitary air-conditioning and air-source heat pump equipment, ANSI/ARI 210/240, Arlington, VA, 1989.

[5] Air-conditioning and Refrigeration Institute, Unitary air-conditioning and air-source heat pump equipment, ANSI/ARI 210/240, Arlington, VA, 2003.

[6] Winandy E., Saavedra C. and Lebrun J., "Experimental analysis and simplified modeling of a hermetic scroll refrigeration compressor", *Applied Thermal Engineering*, v 22, Feb 2002.

[7] Beeton W. and Pham H.M., "Vapor injected scroll compressors", *ASHRAE Journal* April 2003

[8] Elson J.P., private communication regarding efficiency of ZF18K4E-T5F compressor, *Copeland Compressors*, Sidney, OH, Feb 2003.

[9] Park, Youn Cheol, private communication regarding speed and isentropic efficiency characteristics of scroll compressors, Oct 2002.

Appendix A: Results with New Expression for Cycling Loss Factor

The new expression for C_d suggests that the cycling losses are only of the order of 10%. Hence instead of incorporating a costly variable speed drive compressor, it probably might be better to use two single speed compressors working in tandem, as can be shown in the Figure 1

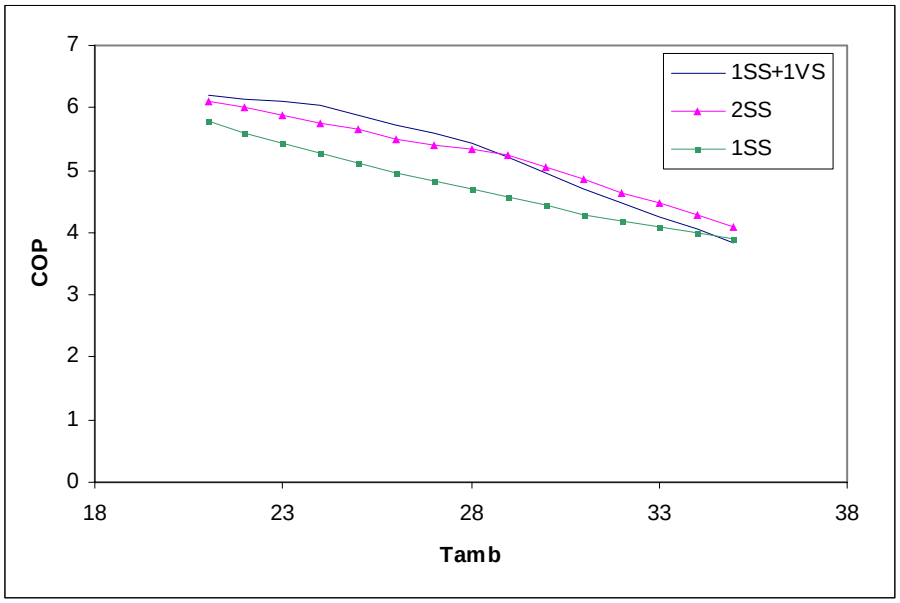

Figure A.1 Comparison between different tandem configurations

From the Figure A.1, it can be noticed, that in the T_{amb} range (21-28°C), the first configuration (1VS+1SS) has a higher COP than the second one (2 equally sized SS). This is because of the fact that the cycling losses are more than the 4% penalty of the variable speed compressor. However in the T_{amb} range (28-35°C), the cycling losses are low, and hence the 2 SS option proves to be more efficient.

Appendix B: Ideal and Real Cycle Comparison

The following Figures B.1 and B.2 illustrate that the ideal HX cycle is identical to the ideal FT cycle. For both the cases we try to identify the location of the injection port, which would result in the maximum COP, and notice that for both the cases we get the peak at the same pressure and a similar curve profile.

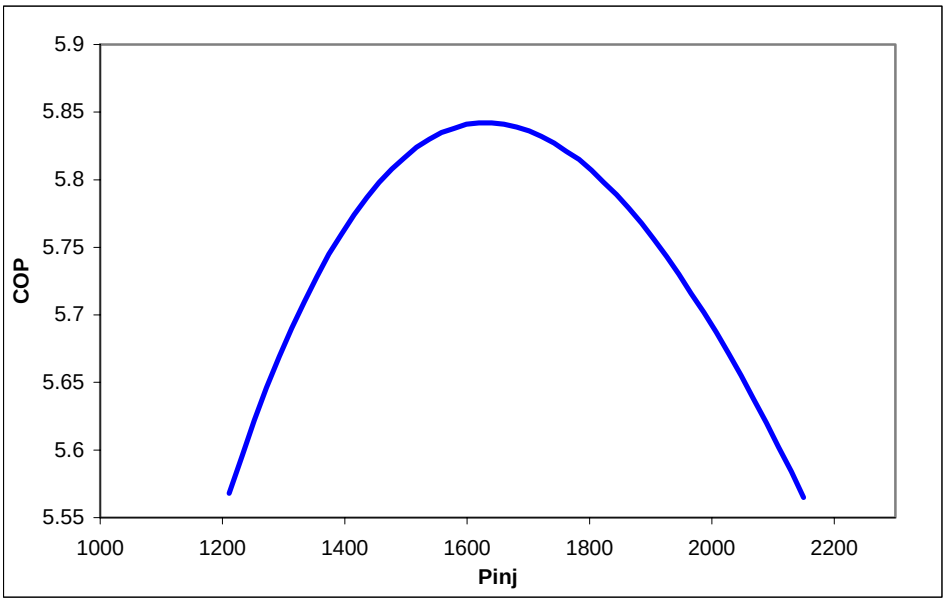

Figure B.1 COP curve as a function of injected pressure for an ideal FT for T_{amb}=28°C (ARI-B)

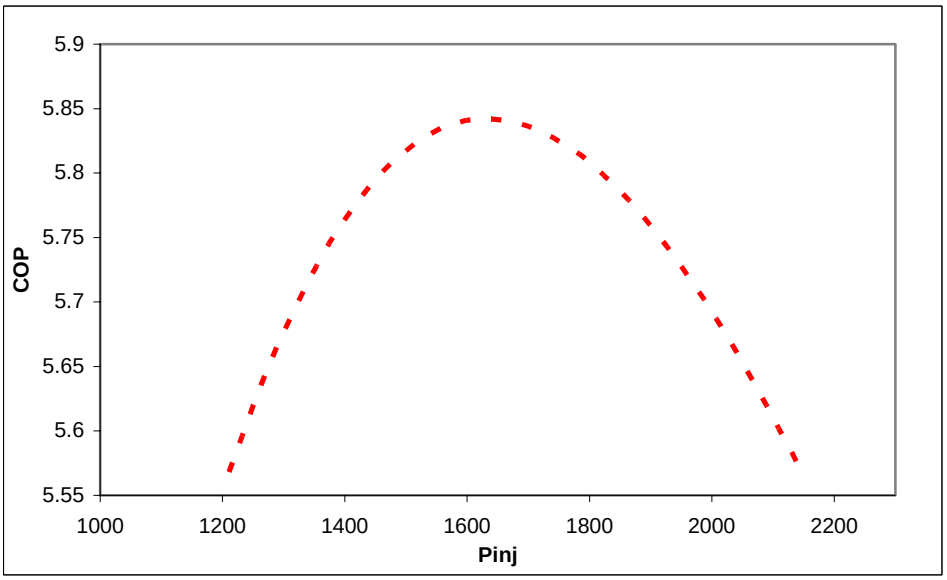

Figure B.2 COP curve as a function of injected pressure for an ideal HX for T_{amb}=28°C (ARI-B)

Figures B.3 and B.4 show how non-ideal flash tanks and heat exchangers can affect cycle COP. For both components, the effects of non-ideal performance are quite small, suggesting that efficient VI systems can be designed to be reasonably compact.

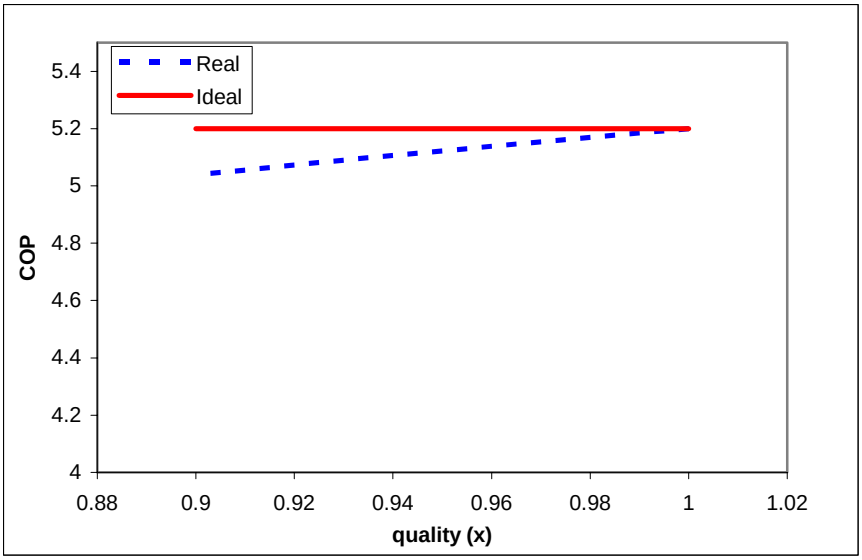

Figure B.3 COP comparison for real FT system with the ideal case.

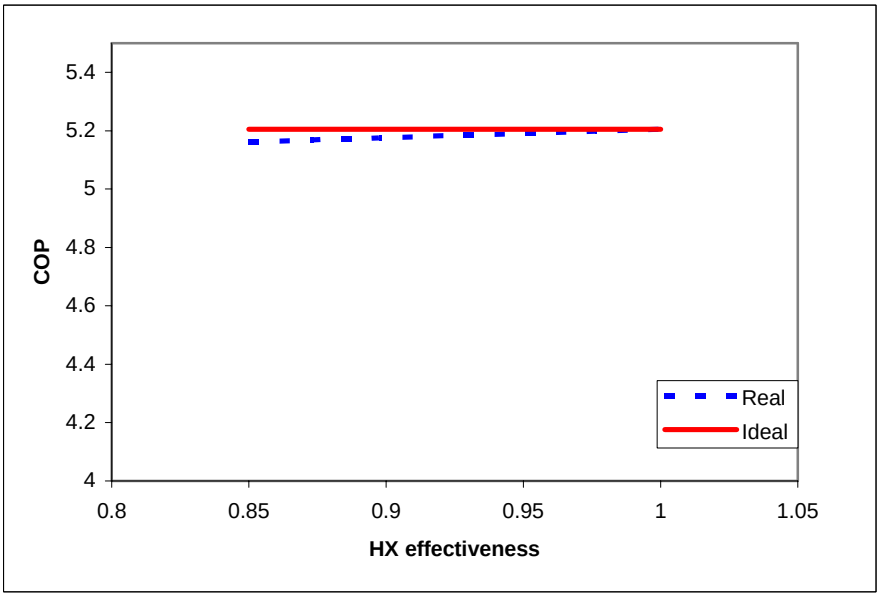

Figure B.4 COP comparison for real HX system with the ideal case.

Figure B.5 shows that the capacity of the system falls by only about 2.5% if we use a HX of effectiveness equal to 0.85 (Figure. 15). Similarly, the capacity of the system also shows a drop of only 3%, if a HX with an effectiveness of 0.85 is used.

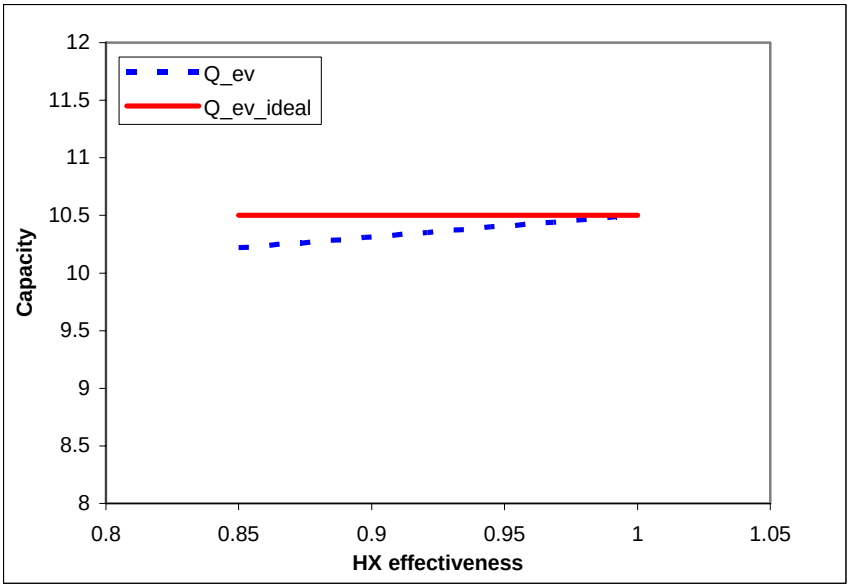

Figure B.5 Capacity comparison for real HX system with the base case

Appendix C: Newer Developments in Compressor Technology

In the above analysis, we had considered the over and under compression model for the scroll compressor. However, the newer version of the scroll compressor comes equipped with a dynamic valve, which prevents over-compression. The system is then modeled taking this fact into consideration and the results are obtained. The cycle characteristics remain almost the same, with the COP increasing by around 6-8% in case of the VI applications, as is shown in the Figure B. The curves do not have a point of inflexion, which shows that we do not have any over-compression.

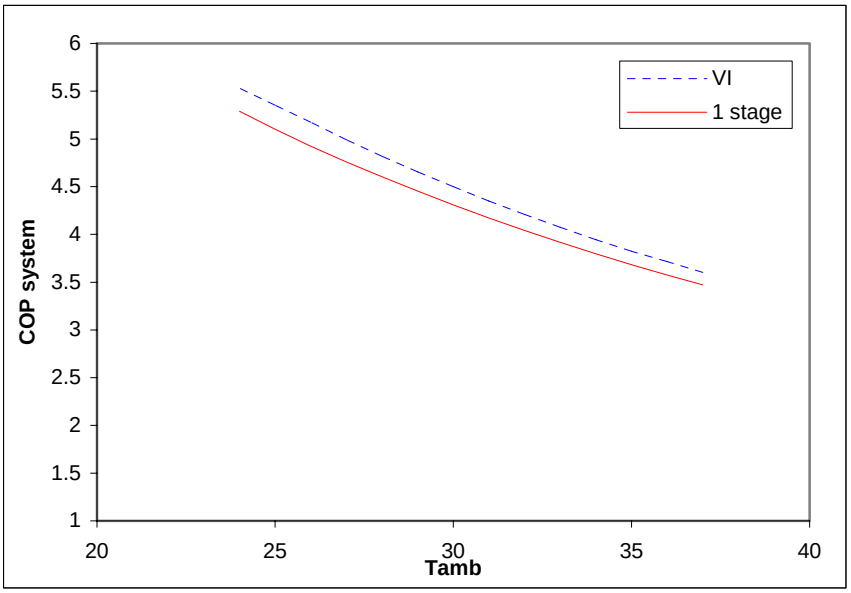

Figure C.1 Comparison between VI and base case with dynamic valve present in a/c applications

Similarly, due to the recent advances made in the compressor technology, the cycling losses have been brought down considerably (*ARI Standards,* 2003), and the newer expression for the multiplicative factor C_d applied to the COP term is shown as below.

$$C_d = 0.9 + 0.1 * \mu$$

Using this expression in our analysis, shows that the COP of the VI system is higher than that of the base case by around 5~7% in the load range (22-37°C). The slight drop in the COP gain (from 6% to 5%) appears because of the new expression for C_d.

Appendix D: Effect of Refrigerant Choice

The preceding analysis focused on R410A as the refrigerant. Using VI systems with different refrigerants like R134a and R22 was also analyzed. Simulation results for these cases are shown in Figures D.1 and D.2 (for a/c applications in the T_{amb} range of 20-40°C). The curves show that similar COP gains were observed for these refrigerants as well.

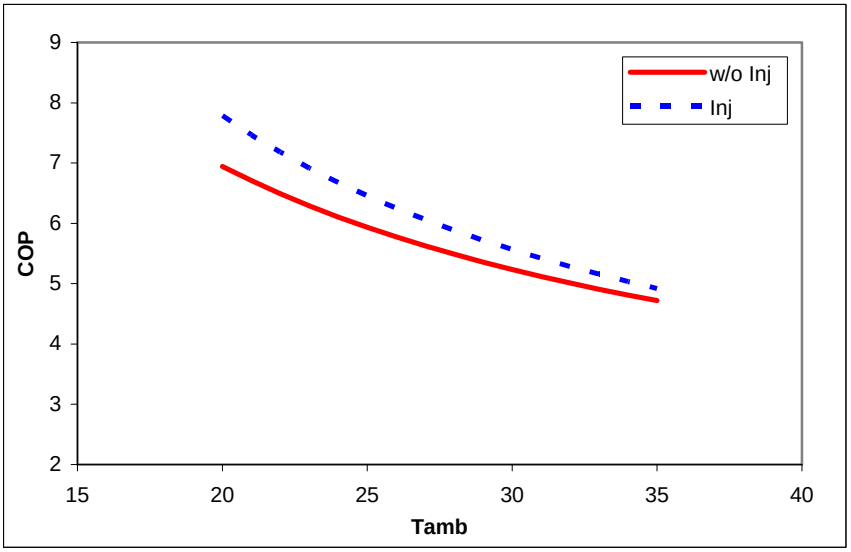

Figure D.1 COP comparison for cases with and without injection for R134a

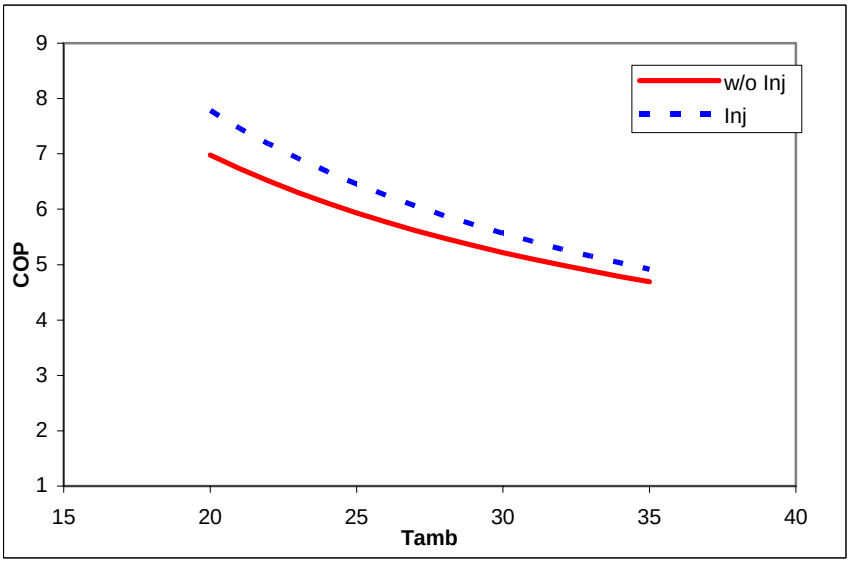

Figure D.2 COP comparison for cases with and without injection for R22